JOURNAL OF APPLIED CRYSTALLOGRAPHY
ISSN 1600-5767

Generalized resolution matrix for neutron spin-echo three-axis spectrometers

Felix Groitl,[a]‡ Thomas Keller[b,c] and Klaus Habicht[a,d]*

[a]Helmholtz-Zentrum Berlin für Materialien und Energie GmbH, 14109 Berlin, Germany, [b]Max Planck Institute for Solid State Research, 70569 Stuttgart, Germany, [c]Max Planck Society Outstation at the FRM II, 85748 Garching, Germany, and [d]Institut für Physik und Astronomie, Universität Potsdam, 14476 Potsdam, Germany. *Correspondence e-mail: habicht@helmholtz-berlin.de

Received 10 November 2017
Accepted 3 April 2018

Edited by G. J. McIntyre, Australian Centre for Neutron Scattering, Australia

‡ Present address: École Polytechnique Fédérale de Lausanne, 1015 Lausanne, Switzerland, and Paul Scherrer Institute, 5232 Villigen PSI, Switzerland.

Keywords: neutron spin-echo; neutron resonance spin-echo spectroscopy; resolution matrix; triple-axis spectroscopy.

This article describes the energy resolution of spin-echo three-axis spectrometers (SE-TASs) by a compact matrix formalism. SE-TASs allow one to measure the line widths of elementary excitations in crystals, such as phonons and magnons, with an energy resolution in the μeV range. The resolution matrices derived here generalize prior work: (i) the formalism works for all crystal structures; (ii) spectrometer detuning effects are included; these arise typically from inaccurate knowledge of the excitation energy and group velocity; (iii) components of the gradient vector of the dispersion surface dω/d$\mathbf{q}$ perpendicular to the scattering plane are properly treated; (iv) the curvature of the dispersion surface is easily calculated in reciprocal units; (v) the formalism permits analysis of spin-echo signals resulting from multiple excitation modes within the three-axis spectrometer resolution ellipsoid.

1. Introduction

Neutron triple-axis spectrometers (TASs) are traditionally used to measure dispersion relations of elementary excitations in single crystals (Shirane *et al.*, 2002). The energy resolution of TASs is a few per cent of the incident neutron energy, which is sufficient to determine the energy of an excitation but not its intrinsic line width. This limitation of TASs was overcome by a proposal of Mezei (1978, 1980) to combine a spin-echo spectrometer consisting of precession devices (PDs) up- and downstream of the sample with the TAS. Inside these PDs, the neutron spins undergo Larmor precession, and the net precession angle after passing both PDs is proportional to the energy transfer $\hbar\omega$ (Fig. 1). In practice, such a combined spin-echo triple-axis spectrometer (SE-TAS) boosts the bare TAS energy resolution by two orders of magnitude. The cost of this improved energy resolution is a loss of intensity, as the spin-echo technique requires the neutron beam to be polarized and analysed.

For a spin-echo measurement, the TAS resolution volume, usually approximated by an ellipsoid in ($\mathbf{Q}$, ω) space, is placed onto the excitation of interest (Fig. 2). The TAS then works as a so-called background spectrometer defining the momentum resolution and a coarse energy resolution; the latter helps to suppress background. The spin-echo part is shown as planes of constant phase (PCP), where all scattering events lying on such a plane get the same net Larmor phase, and parallel planes correspond to constant phase differences. If these planes are tuned to be parallel to the dispersion surface, the phase differences $\Delta\Phi$ of scattering events encode the intrinsic energy width of the excitation. This tuning is achieved by

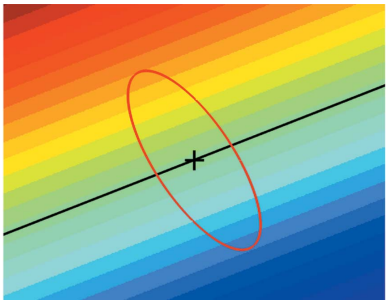

selecting appropriate magnitudes of the magnetic fields $B_{1,2}$ and the inclination angles $\theta_{1,2}$ of the field boundaries of the PDs. As the PCP are flat, whereas the dispersion surface in general is curved, a finite energy resolution is introduced, corresponding to the deviation between planes and dispersion within the volume of the ellipsoid.

Present SE-TASs take advantage of the resonance spin-echo technique to implement the PDs (Golub & Gähler, 1987; Gähler & Golub, 1988). Neutron resonance spin-echo (NRSE) is based on small radiofrequency spin-flip coils to define the boundaries of the PDs. Inclination of the boundaries is achieved by rotating these coils. The first instrument based on this technique is FLEX-NRSE, which allows one to measure line widths of elementary excitations over broad ranges of momentum and energy transfer with an energy resolution as low as 1 μeV. That is roughly two orders of magnitude better than on conventional neutron spectrometers. The first line-width studies included phonons and rotons in superfluid ^{4}He (Keller *et al.*, 2004), phonon anharmonicities in Pb (Habicht *et al.*, 2004) and magnon–magnon scattering in the model Heisenberg antiferromagnet MnF_2 (Bayrakci *et al.*, 2006). The data for the latter experiment were completed at the NRSE-TAS instrument TRISP at the FRM II (Keller, Habicht *et al.*, 2002), which was constructed on the basis of the FLEX design. A second NRSE-TAS instrument using the FLEX-NRSE design with modified radiofrequency flippers is ZETA at the ILL (Klimko *et al.*, 2003; Martin *et al.*, 2011). Recently, a new design of the PDs based on superconducting magnetic Wallaston prisms reached a performance comparable to that of NRSE (Li *et al.*, 2017). These prisms are more compact than the current NRSE designs and can be easily integrated in existing polarized TAS instruments.

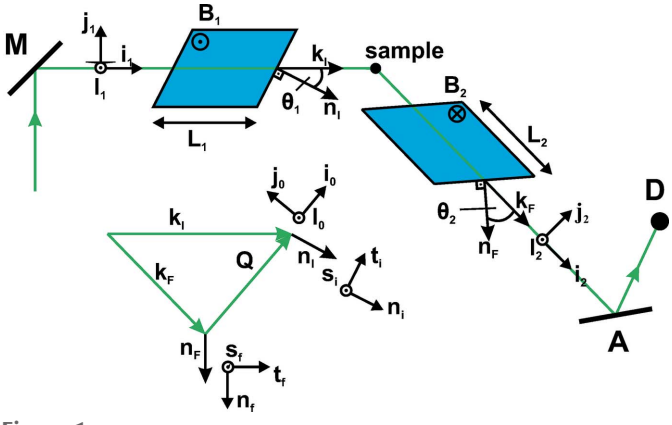

Figure 1
Spin-echo triple-axis spectrometer layout. M and A are the TAS monochromator and analyser, respectively, defining $\mathbf{k}_{I,F}$, and D is the detector. The precession devices (PDs, blue regions) provide DC fields $\mathbf{B}_{1,2}$ and boundaries with inclination angles $\theta_{1,2}$. Several coordinate systems are used in the calculations: $\mathbf{i}_{1,2} \parallel \mathbf{k}_{I,F}$, $\mathbf{j}_{1,2} \perp \mathbf{k}_{I,F}$ in the scattering plane, $\mathbf{l}_{1,2}$ perpendicular to the scattering plane. The inset shows the scattering triangle $\mathbf{Q} = \mathbf{k}_I - \mathbf{k}_F$, where $\mathbf{Q}$ is expressed in coordinates $\mathbf{i}_0 \parallel \mathbf{Q}, \mathbf{j}_0 \perp \mathbf{Q}$ in the scattering plane, $\mathbf{i}_0$ perpendicular to the scattering plane. The vectors $\mathbf{n}_{I,F}$ normal to the field boundaries are described in coordinates $\mathbf{n}_{i,f} \parallel \mathbf{n}_{I,F}$, $\mathbf{t}_{i,f} \perp \mathbf{n}_{I,F}$ in the scattering plane, and $\mathbf{s}_{i,f}$ perpendicular to the scattering plane.

An adequate description of the energy resolution of SE-TASs is needed both for planning experiments and for the data analysis. A compact resolution matrix formalism based on a second-order expansion of all relevant parameters, including the TAS resolution, the curvature of the dispersion surface, and the spread of both the crystal mosaicity and lattice spacing, is available (Habicht *et al.*, 2003). However, this formalism is limited to tuned instruments, meaning that the TAS resolution ellipsoid is centred on the excitation ($\mathbf{q}_0$, ω_0), and the PCP are perfectly tangential to the dispersion surface at this point. Detuning effects are included in the generalized formalism presented in this work. These effects typically arise from inaccurate values of the energy and the group velocity of an excitation, such that the TAS ellipsoid is not centred on the excitation and the PCP are not properly aligned. The formalism then allows one to calculate the accuracy of the spin-echo linewidth data on the basis of an error estimate of the dispersion parameters. Unavoidable detuning effects occur if several dispersion branches with different energies and/or group velocities appear within the volume of the TAS resolution ellipsoid, for example if multiple modes are split or otherwise not well separated. It is not possible to tune the instrument to all modes and the detuning that arises can be described with the new formalism. A first application was the analysis of split magnon branches emerging from two misaligned crystallites (Habicht *et al.*, 2010). The new formalism was also tested on split phonon modes from crystals with controllable misalignment.

The current work further extends the formalism presented by Habicht *et al.* (2010). After a brief summary of the basic spin-echo equations we derive the generalized resolution matrix, where all relevant parameters are expanded to second order and are assumed to follow Gaussian distributions. We apply the resolution matrix to a few practical cases and to experimental results on model systems.

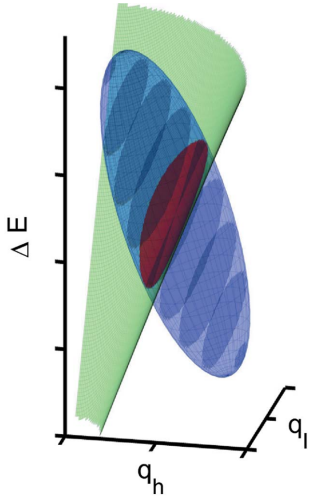

Figure 2
The TAS resolution ellipsoid (blue) cuts a small section (red) of the curved dispersion surface (green). The planes of constant SE phase (PCP, dark blue) are parallel to a plane oriented tangentially to the dispersion surface.

2. Resolution matrix

2.1. Simplified model of SE-TASs

We first give a brief summary of the SE-TAS resolution properties, where we assume perfect PDs with uniform fields (without fringing fields). The normal vectors $\mathbf{n}_{\rm i,f}$ are within the scattering plane defined by $\mathbf{k}_{\rm I,F}$. In a later step we will allow for arbitrary inclination of the PD boundaries. We further assume that there is only one dispersion surface within the TAS resolution ellipsoid and that the ellipsoid is centred on the point $(\mathbf{q}_0, \omega_0)$ on this dispersion. Later, we will generalize the formalism to allow for more than one dispersion surface and an off-centred resolution ellipsoid.

The basic setup and all coordinate systems are shown in Fig. 1. The incident and scattered neutrons have mean wavenumbers $\mathbf{k}_{\rm I,F}$, indicated by capital indices. The PDs provide uniform magnetic fields $\mathbf{B}_{1,2}$ of length $L_{1,2}$ with boundary inclination angles $\theta_{1,2}$. Positive angles correspond to counterclockwise rotation. In this article, we give the polarization P as a complex number. The physical polarization of the neutron beam is the real part Re(P) and the magnitude $|P|$ is the so-called echo amplitude. P downstream of the second PD is

$$P = \frac{1}{N}\int S(\mathbf{Q},\omega) R_{\rm TAS}(\mathbf{k}_{\rm i},\mathbf{k}_{\rm f}) \exp[i\Phi(\mathbf{k}_{\rm i},\mathbf{k}_{\rm f})]\, {\rm d}^3k_{\rm i}\, {\rm d}^3k_{\rm f}, \quad (1)$$

where $S(\mathbf{Q},\omega)$ is the scattering function, $R_{\rm TAS}(\mathbf{k}_{\rm i},\mathbf{k}_{\rm f})$ is the TAS transmission function, N is a normalization constant and $\Phi(\mathbf{k}_{\rm i},\mathbf{k}_{\rm f})$ is the net Larmor phase:

$$\begin{aligned}\Phi(\mathbf{k}_{\rm i},\mathbf{k}_{\rm f}) &= \Phi_0(\mathbf{k}_{\rm I},\mathbf{k}_{\rm F}) + \Delta\Phi(\Delta\mathbf{k}_{\rm i},\Delta\mathbf{k}_{\rm f}) \\ &= \frac{A_1}{\mathbf{k}_{\rm i}\cdot\mathbf{n}_{\rm I}} - \frac{A_2}{\mathbf{k}_{\rm f}\cdot\mathbf{n}_{\rm F}} \end{aligned} \quad (2)$$

with $A_{1,2} = (m/\hbar)\omega_{L1,2}L_{1,2}\cos\theta_{1,2}$, the neutron mass m, the Larmor frequency $\omega_{L1,2} = \gamma B_{1,2}$ and the gyromagnetic ratio of the neutron $\gamma = 2\pi \times 2.916$ kHz G^{-1}. We treat the Larmor precession in a classical way; a quantum mechanical treatment is given by Gähler *et al.* (1998), Keller, Golub *et al.* (2002) and Habicht (2003). The actual wavenumber $\mathbf{k}_{\rm i,f}$ of a neutron deviates from the mean: $\mathbf{k}_{\rm i,f} = \mathbf{k}_{\rm I,F} + \Delta\mathbf{k}_{\rm i,f}$. Further, we use the conventional definitions $\mathbf{Q}_0 = \mathbf{q}_0 + \mathbf{G}_0 = \mathbf{k}_{\rm I} - \mathbf{k}_{\rm F}$ and $\omega_0 = \omega(\mathbf{q}_0) = \hbar/2m(\mathbf{k}_{\rm I}^2 - \mathbf{k}_{\rm F}^2)$, where $\mathbf{q}_0$ is the momentum of the excitation and $\mathbf{G}_0$ is a reciprocal-lattice vector.

The spin-echo (SE) tuning conditions for the PD inclination angles and field ratio are obtained from a first-order expansion of the Larmor phase [see equation (2)]:

$$\mathbf{n}_{\rm I,F} = \frac{(\hbar/m)\mathbf{k}_{\rm I,F} - \nabla_{\mathbf{q}}\omega_0(\mathbf{q}_0)}{N_{\rm I,F}}, \quad (3)$$

$$\frac{\omega_{L1}L_1}{\omega_{L2}L_2} = \frac{\cos\Theta_2(\mathbf{k}_{\rm I}\cdot\mathbf{n}_{\rm I})^2 N_{\rm I}}{\cos\Theta_1(\mathbf{k}_{\rm F}\cdot\mathbf{n}_{\rm F})^2 N_{\rm F}}, \quad (4)$$

with

$$N_{\rm I,F} = \left|\frac{\hbar}{m}\mathbf{k}_{\rm I,F} - \nabla_{\mathbf{q}}\omega_0(\mathbf{q}_0)\right|. \quad (5)$$

The so-called SE time τ is given by

$$\tau = \frac{A_{1,2}}{(\mathbf{k}_{\rm I,F}\cdot\mathbf{n}_{\rm I,F})^2 N_{\rm I,F}}. \quad (6)$$

If the tuning conditions (3) and (4) are satisfied, the simple relation $\Delta\Phi = \tau\,\Delta\omega$ holds, where $\Delta\omega = 0$ is defined by a plane of constant Larmor phase tangential to the dispersion sheet. The value for τ from equation (6) is then the same for the two PDs.

2.2. Second-order expansion of the SE phase

For a general calculation of the resolution function, we expand the phase [equation (2)] to second order in $\Delta\mathbf{k}_{\rm i,f}$ and $\Delta\omega$. The TAS resolution ellipsoid will be described by including the matrix elements derived by Popovici (1975) and Stoica (1975). The calculation follows Habicht *et al.* (2003), but we allow for the following generalizations: (i) The SE might be detuned; this means equations (3) and (4) are not satisfied. This includes a detuning of the TAS in the sense that the resolution ellipsoid is not centred at the nominal excitation $(\mathbf{q}_0, \omega_0)$. (ii) There are no restrictions to the crystallographic symmetry of the sample crystal. All vectors in the following calculations are assumed to be expressed in Cartesian coordinates, which are related to the crystal lattice by the **UB** matrix formalism (Lumsden *et al.*, 2005). (iii) The local gradient of the dispersion surface $\nabla\omega(\mathbf{q}_0)$ may have components perpendicular to the scattering plane.

The Larmor phase [equation (2)] expanded to second order is

$$\begin{aligned}&\Phi(\mathbf{k}_{\rm i},\mathbf{k}_{\rm f}) - \Phi_0 = \\ &-\frac{A_1}{(\mathbf{k}_{\rm I}\cdot\mathbf{n}_{\rm i})^2}(\Delta\mathbf{k}_{\rm i}\cdot\mathbf{n}_{\rm i}) + \frac{A_2}{(\mathbf{k}_{\rm F}\cdot\mathbf{n}_{\rm f})^2}(\Delta\mathbf{k}_{\rm f}\cdot\mathbf{n}_{\rm f}) \\ &+\frac{A_1}{(\mathbf{k}_{\rm I}\cdot\mathbf{n}_{\rm i})^3}(\Delta\mathbf{k}_{\rm i}\cdot\mathbf{n}_{\rm i})^2 - \frac{A_2}{(\mathbf{k}_{\rm F}\cdot\mathbf{n}_{\rm f})^3}(\Delta\mathbf{k}_{\rm f}\cdot\mathbf{n}_{\rm f})^2. \end{aligned} \quad (7)$$

The aim is to express the total Larmor precession angle in terms of the vector $\mathbf{J} = (\Delta\omega, \Delta k_{\rm in}, y_1, y_2, z_1, z_2)$ with

$$\Delta\mathbf{k}_{\rm i} = x_1\mathbf{i}_1 + y_1\mathbf{j}_1 + z_1\mathbf{l}_1, \quad (8)$$

$$\Delta\mathbf{k}_{\rm f} = x_2\mathbf{i}_2 + y_2\mathbf{j}_2 + z_2\mathbf{l}_2, \quad (9)$$

$$\Delta k_{\rm in} = \Delta\mathbf{k}_{\rm i}\cdot\mathbf{n}_{\rm i}. \quad (10)$$

As a next step we expand the dispersion relation. Here we have to include both the curvature of the dispersion surface and variations of the reciprocal-lattice vector **G** arising from sample imperfections, that is the mosaicity and a spread of the lattice spacing of the sample crystal. Both effects are treated in detail in §§2.4 and 2.5. At this point of the calculation, we anticipate the definition of a curvature matrix $\mathbf{H}_0$, which incorporates the second derivatives of the dispersion surface. Expanding the dispersion relation to second order we obtain

$$\omega(\mathbf{q}) = \omega(\mathbf{q}_0) + \Delta\omega + \Delta\mathbf{q}\cdot\nabla\omega(\mathbf{q}_0) + \frac{1}{2}\Delta\mathbf{q}^{\rm T}\mathbf{H}_0\Delta\mathbf{q} \quad (11)$$

with $\mathbf{q} = \mathbf{q}_0 + \Delta\mathbf{q}$, $\mathbf{q}_0 + \mathbf{G}_0 = \mathbf{k}_{\rm I} - \mathbf{k}_{\rm F}$ and $\Delta\mathbf{q} = \Delta\mathbf{k}_{\rm i} - \Delta\mathbf{k}_{\rm i}$. We assume that the line width of the excitation is constant within the volume of the TAS resolution ellipsoid, such that

$\Delta\omega$ does not depend on $\mathbf{q}$. The reciprocal-lattice vector $\mathbf{G}$ varies around $\mathbf{G}_0$ owing to sample imperfections, including the mosaic spread and variations in the lattice spacing corresponding to a variation of the magnitude and direction of $\mathbf{G}$, respectively:

$$\mathbf{G} = \mathbf{G}_0 + \Delta\mathbf{G}. \tag{12}$$

Since the momentum transfer is defined as

$$\mathbf{Q} = \mathbf{k}_\mathrm{i} - \mathbf{k}_\mathrm{f} = \mathbf{G} + \mathbf{q} \tag{13}$$

the lattice imperfections $\Delta\mathbf{G}$ lead to an additional variation of the wavevector:

$$\Delta\mathbf{q}' = \Delta\mathbf{q} - \Delta\mathbf{G} = \Delta\mathbf{k}_\mathrm{i} - \Delta\mathbf{k}_\mathrm{f} - \Delta\mathbf{G}. \tag{14}$$

Combining equations (11) and (14) gives

$$\begin{aligned}\omega(\mathbf{q}) = \omega(\mathbf{q}_0) + \Delta\omega + \Delta\mathbf{k}_\mathrm{i}\cdot\nabla\omega(\mathbf{q}_0) - \Delta\mathbf{k}_\mathrm{f}\cdot\nabla\omega(\mathbf{q}_0)\\ - \Delta\mathbf{G}\cdot\nabla\omega(\mathbf{q}_0) + \frac{1}{2}\Delta\mathbf{q}'^{\mathrm{T}}\mathbf{H}_0\Delta\mathbf{q}'.\end{aligned} \tag{15}$$

The energy conservation $\omega(\mathbf{q}_\mathrm{c}) = \hbar/2m(\mathbf{k}_\mathrm{i}^2 - \mathbf{k}_\mathrm{f}^2)$ expanded to second order reads

$$\omega(\mathbf{q}) = \omega(\mathbf{q}_0) + \frac{\hbar}{m}\mathbf{k}_\mathrm{I}\cdot\Delta\mathbf{k}_\mathrm{i} - \frac{\hbar}{m}\mathbf{k}_\mathrm{F}\cdot\Delta\mathbf{k}_\mathrm{f} + \frac{\hbar}{2m}\Delta\mathbf{k}_\mathrm{i}^2 - \frac{\hbar}{2m}\Delta\mathbf{k}_\mathrm{f}^2. \tag{16}$$

Combining equations (15) and (16) yields

$$\begin{aligned}\Delta\omega = \left[\frac{\hbar}{m}\mathbf{k}_\mathrm{I} - \nabla\omega(\mathbf{q}_0)\right]\cdot\Delta\mathbf{k}_\mathrm{i} + \frac{\hbar}{2m}\Delta\mathbf{k}_\mathrm{i}^2 - \frac{\hbar}{2m}\Delta\mathbf{k}_\mathrm{f}^2\\ - \left[\frac{\hbar}{m}\mathbf{k}_\mathrm{F} - \nabla\omega(\mathbf{q}_0)\right]\cdot\Delta\mathbf{k}_\mathrm{f} + \Delta\mathbf{G}\cdot\nabla\omega(\mathbf{q}_0)\\ - \frac{1}{2}\Delta q'^{\mathrm{T}}\mathbf{H}_0\Delta\mathbf{q}'.\end{aligned} \tag{17}$$

In the next step we allow for detuning both the field ratio and the inclination angles of the PDs. Then equation (6) yields different values for the two PDs:

$$\tau_{1,2} = \frac{A_{1,2}}{\left(\mathbf{k}_\mathrm{I,F}\cdot\mathbf{n}_\mathrm{i,f}\right)^2 N_\mathrm{I,F}}. \tag{18}$$

To obtain the relevant second-order terms, we first multiply equation (17) with τ_2:

$$\begin{aligned}\tau_2\Delta\omega &= \frac{A_2}{(\mathbf{k}_\mathrm{F}\cdot\mathbf{n}_\mathrm{f})^2 N_\mathrm{F}}\left[\frac{\hbar}{m}\mathbf{k}_\mathrm{I} - \nabla\omega(\mathbf{q}_0)\right]\cdot\Delta\mathbf{k}_\mathrm{i}\\ &\quad - \frac{A_2}{(\mathbf{k}_\mathrm{F}\cdot\mathbf{n}_\mathrm{f})^2}\frac{(\hbar/m)\mathbf{k}_\mathrm{F} - \nabla\omega(\mathbf{q}_0)}{N_\mathrm{F}}\cdot\Delta\mathbf{k}_\mathrm{f}\\ &\quad + \frac{\hbar}{2m}\tau_2\Delta\mathbf{k}_\mathrm{i}^2 - \frac{\hbar}{2m}\tau_2\Delta\mathbf{k}_\mathrm{f}^2 + \tau_2\Delta\mathbf{G}\cdot\nabla\omega(\mathbf{q}_{\mathrm{c}0})\\ &\quad - \frac{1}{2}\tau_2\Delta\mathbf{q}'^{\mathrm{T}}\mathbf{H}_0\Delta\mathbf{q}'\\ &= \frac{A_2}{(\mathbf{k}_\mathrm{F}\cdot\mathbf{n}_\mathrm{f})^2}\frac{N_\mathrm{I}}{N_\mathrm{F}}\boldsymbol{\varepsilon}_\mathrm{i}\cdot\Delta\mathbf{k}_\mathrm{i} - \frac{A_2}{(\mathbf{k}_\mathrm{F}\cdot\mathbf{n}_\mathrm{f})^2}\boldsymbol{\varepsilon}_\mathrm{f}\cdot\Delta\mathbf{k}_\mathrm{f}\\ &\quad + \frac{\hbar}{2m}\tau_2\Delta\mathbf{k}_\mathrm{i}^2 - \frac{\hbar}{2m}\tau_2\Delta\mathbf{k}_\mathrm{f}^2 + \tau_2\Delta\mathbf{G}\cdot\nabla\omega(\mathbf{q}_0)\\ &\quad - \frac{1}{2}\tau_2\Delta\mathbf{q}'^{\mathrm{T}}\mathbf{H}_0\Delta\mathbf{q}'.\end{aligned} \tag{19}$$

We define the unit vectors

$$\boldsymbol{\varepsilon}_\mathrm{i,f} = \frac{(\hbar/m)\mathbf{k}_\mathrm{I,F} - \nabla\omega(\mathbf{q}_{\mathrm{c}0})}{N_\mathrm{I,F}} \tag{20}$$

with the components $e_{\mathrm{i,f}1}, e_{\mathrm{i,f}2}, e_{\mathrm{i,f}3}$ in the coordinates defined in Fig. 1:

$$e_{\mathrm{i}1,\mathrm{f}1} = \boldsymbol{\varepsilon}_\mathrm{i,f}\cdot\mathbf{n}_\mathrm{i,f}, \quad e_{\mathrm{i}2,\mathrm{f}2} = \boldsymbol{\varepsilon}_\mathrm{i,f}\cdot\mathbf{t}_\mathrm{i,f}, \quad e_{\mathrm{i}3,\mathrm{f}3} = \boldsymbol{\varepsilon}_\mathrm{i,f}\cdot\mathbf{s}_\mathrm{i,f}. \tag{21}$$

Inserting equation (21) in equation (19) yields

$$\begin{aligned}\frac{A_2}{(\mathbf{k}_\mathrm{F}\cdot\mathbf{n}_\mathrm{f})^2}\Delta\mathbf{k}_\mathrm{f}\cdot\mathbf{n}_\mathrm{f} &= -\tau_2''\Delta\omega + \tau_2''N_\mathrm{I}e_{\mathrm{i}1}\Delta k_\mathrm{in}\\ &\quad + \tau_2''N_\mathrm{I}e_{\mathrm{i}2}\left(-\Delta k_\mathrm{in}\tan\theta_1 + y_1\frac{1}{\cos\theta_1}\right)\\ &\quad + \tau_2''N_\mathrm{I}e_{\mathrm{i}3}z_1 - \tau_2''N_\mathrm{F}e_{\mathrm{f}3}z_2\\ &\quad - \tau_2''N_\mathrm{F}e_{\mathrm{f}2}\frac{1}{\cos\theta_2}y_2 + \frac{\hbar}{2m}\tau_2''\Delta\mathbf{k}_\mathrm{i}^2\\ &\quad - \frac{\hbar}{2m}\tau_2''\Delta\mathbf{k}_\mathrm{f}^2 + \tau_2''\Delta\mathbf{G}\cdot\nabla\omega(\mathbf{q}_0)\\ &\quad - \frac{1}{2}\tau_2''\Delta\mathbf{q}'^{\mathrm{T}}\mathbf{H}_0\Delta\mathbf{q}'\end{aligned} \tag{22}$$

with

$$\tau_2'' = \frac{\tau_2}{(e_\mathrm{f1} - e_\mathrm{f2}\tan\theta_2)}. \tag{23}$$

In deriving equation (22) the following relations for $\Delta\mathbf{k}_\mathrm{i,f}$ expressed in the basis of $\mathbf{n}_\mathrm{i,f}$, $\mathbf{t}_\mathrm{i,f}$ and $\mathbf{s}_\mathrm{i,f}$ were used:

$$\mathbf{s}_\mathrm{i}\cdot\Delta\mathbf{k}_\mathrm{i} = z_1, \tag{24}$$

$$\mathbf{s}_\mathrm{f}\cdot\Delta\mathbf{k}_\mathrm{f} = z_2, \tag{25}$$

$$\mathbf{n}_\mathrm{i}\cdot\Delta\mathbf{k}_\mathrm{i} = \Delta k_\mathrm{in}, \tag{26}$$

$$\begin{aligned}\Delta\mathbf{k}_\mathrm{i} &= (x_1\cos\theta_1 + y_1\sin\theta_1)\mathbf{n}_\mathrm{i}\\ &\quad + (-x_1\sin\theta_1 + y_1\cos\theta_1)\mathbf{t}_\mathrm{i} + z_1\mathbf{s}_\mathrm{i}\\ &= \Delta k_\mathrm{in}\mathbf{n}_\mathrm{i} + \left(-\Delta k_\mathrm{in}\tan\theta_1 + y_1\frac{1}{\cos\theta_1}\right)\mathbf{t}_\mathrm{i} + z_1\mathbf{s}_\mathrm{i},\end{aligned} \tag{27}$$

$$\Delta\mathbf{k}_\mathrm{f} = (\Delta\mathbf{k}_\mathrm{f}\cdot\mathbf{n}_\mathrm{f})\mathbf{n}_\mathrm{f} + \left[-(\Delta\mathbf{k}_\mathrm{f}\cdot\mathbf{n}_\mathrm{f})\tan\theta_2 + y_2\frac{1}{\cos\theta_2}\right]\mathbf{t}_\mathrm{f} + z_2\mathbf{s}_\mathrm{f}, \tag{28}$$

$$\mathbf{t}_\mathrm{i}\cdot\Delta\mathbf{k}_\mathrm{i} = -\Delta k_\mathrm{in}\tan\theta_1 + y_1\frac{1}{\cos\theta_1}, \tag{29}$$

$$\mathbf{t}_\mathrm{f}\cdot\Delta\mathbf{k}_\mathrm{f} = -(\Delta\mathbf{k}_\mathrm{f}\cdot\mathbf{n}_\mathrm{f})\tan\theta_2 + y_2\frac{1}{\cos\theta_2}. \tag{30}$$

Substituting equation (22) into equation (7) gives the Larmor phase:

$$\Phi(\mathbf{k}_\mathrm{i},\mathbf{k}_\mathrm{f})-\Phi_0=-\tau_1 N_\mathrm{I}\Delta k_\mathrm{in}-\tau_2''\Delta\omega+\tau_2'' N_\mathrm{I} e_{\mathrm{i}1}\Delta k_\mathrm{in}+\tau_2'' N_\mathrm{I} e_{\mathrm{i}2}\left(-\Delta k_\mathrm{in}\tan\theta_1+y_1\frac{1}{\cos\theta_1}\right)+\tau_2'' N_\mathrm{I} e_{\mathrm{i}3} z_1-\tau_2'' N_\mathrm{F} e_{\mathrm{f}2}\frac{1}{\cos\theta_2}y_2-\tau_2'' N_\mathrm{F} e_{\mathrm{f}3} z_2+\tau_2''\Delta\mathbf{G}\cdot\nabla\omega(\mathbf{q}_0)-\frac{1}{2}\tau_2''\Delta\mathbf{q}'^{\mathrm{T}}\mathbf{H}_0\Delta\mathbf{q}'+\frac{\hbar}{2m}\tau_2''\Delta\mathbf{k}_\mathrm{i}^2-\frac{\hbar}{2m}\tau_2''\Delta\mathbf{k}_\mathrm{f}^2+\tau_1\frac{N_\mathrm{I}}{\mathbf{k}_\mathrm{I}\cdot\mathbf{n}_\mathrm{i}}\Delta k_\mathrm{in}^2-\tau_2\frac{N_\mathrm{F}}{\mathbf{k}_\mathrm{F}\cdot\mathbf{n}_\mathrm{f}}(\Delta\mathbf{k}_\mathrm{f}\cdot\mathbf{n}_\mathrm{f})^2. \quad (31)$$

This expression of the Larmor phase includes second-order terms with the above-mentioned generalizations.

The term $(\Delta\mathbf{k}_\mathrm{f}\cdot\mathbf{n}_\mathrm{f})^2$ in equation (31) is now substituted by using equation (22). Since only second-order effects are considered and higher-order terms are neglected, it is sufficient to use equation (22) to first order only:

$$\Delta\mathbf{k}_\mathrm{f}\cdot\mathbf{n}_\mathrm{f}=-\frac{1}{C_\mathrm{f}N_\mathrm{F}}\Delta\omega+\frac{N_\mathrm{I}C_\mathrm{i}}{N_\mathrm{F}C_\mathrm{f}}\Delta k_\mathrm{in}+\frac{N_\mathrm{I}}{C_\mathrm{f}N_\mathrm{F}}e_{\mathrm{i}2}\frac{1}{\cos\theta_1}y_1-\frac{1}{C_\mathrm{f}}e_{\mathrm{f}2}\frac{1}{\cos\theta_2}y_2+\frac{N_\mathrm{I}}{C_\mathrm{f}N_\mathrm{F}}e_{\mathrm{i}3}z_1-\frac{1}{C_\mathrm{f}}e_{\mathrm{f}3}z_2+\frac{1}{C_\mathrm{f}N_\mathrm{F}}\Delta\mathbf{G}'\cdot\nabla\omega(\mathbf{q}_0) \quad (32)$$

with

$$\tau_2=\frac{A_2}{(\mathbf{k}_\mathrm{f}\cdot\mathbf{n}_\mathrm{f})^2 N_\mathrm{F}}, \quad (33)$$

$$C_\mathrm{i}=e_{\mathrm{i}1}-e_{\mathrm{i}2}\tan\theta_1, \quad (34)$$

$$C_\mathrm{f}=e_{\mathrm{f}1}-e_{\mathrm{f}2}\tan\theta_2. \quad (35)$$

The term $+(1/C_\mathrm{f}N_\mathrm{F})\Delta\mathbf{G}'\cdot\nabla\omega(\mathbf{q}_0)$ considers only the first-order terms arising from the lattice imperfections. This term introduces cross terms between the lattice imperfection variables $\Delta\eta$, $\Delta\nu$ (horizontal and vertical mosaic) and ΔG_c (lattice constant variation) and the variables of the six-component vector $\mathbf{J}$. $\Delta\mathbf{G}'_\mathrm{c}$ is defined in equation (49). $\Delta\mathbf{k}_\mathrm{i}^2$ and $\Delta\mathbf{k}_\mathrm{f}^2$ are substituted in equation (31) using equations (27) and (28):

$$\Delta\mathbf{k}_\mathrm{i}^2=\Delta k_\mathrm{in}^2+\left(-\Delta k_\mathrm{in}\tan\theta_1+y_1\frac{1}{\cos\theta_1}\right)^2+z_1^2, \quad (36)$$

$$\Delta\mathbf{k}_\mathrm{f}^2=(\Delta\mathbf{k}_\mathrm{f}\cdot\mathbf{n}_\mathrm{f})^2+\left[-(\Delta\mathbf{k}_\mathrm{f}\cdot\mathbf{n}_\mathrm{f})\tan\theta_2+y_2\frac{1}{\cos\theta_2}\right]^2+z_2^2. \quad (37)$$

Inserting equations (36) and (37) into equation (31) and using again equation (32) to substitute all $\Delta\mathbf{k}_\mathrm{f}\cdot\mathbf{n}_\mathrm{f}$ terms allows us to express the total Larmor precession angle as a function of squared and cross terms of the six variables $(\Delta\omega, \Delta k_\mathrm{in}, y_1, y_2, z_1, z_2)$. The total Larmor phase can conveniently be expressed in matrix notation:

$$\Phi(\mathbf{k}_\mathrm{i},\mathbf{k}_\mathrm{f})-\Phi_0=\tau_2''\mathbf{T}^\mathrm{T}\mathbf{J}-\frac{1}{2}\tau_2''\mathbf{J}^\mathrm{T}\mathbf{\Psi}\mathbf{J}+\tau_2''\Delta\mathbf{G}\cdot\nabla\omega(\mathbf{q}_0)-\frac{1}{2}\tau_2''\Delta\mathbf{q}'^{\mathrm{T}}\mathbf{H}_0\Delta\mathbf{q}'+X(\Delta\mathbf{G}). \quad (38)$$

Here $X(\Delta\mathbf{G})$ denotes all cross terms introduced by sample imperfections treated in §2.4. The components of the six-dimensional column vector $\mathbf{T}$ and the elements of the symmetric (6×6) matrix $\mathbf{\Psi}$ are given in Appendices *B*1 and *B*2. For the special case, where the SE conditions are satisfied and the gradient $\nabla\omega(\mathbf{q}_0)$ lies in the scattering plane, the components reduce to

$$e_{\mathrm{i}1,\mathrm{f}1}=1, \quad e_{\mathrm{i}2,\mathrm{f}2}=e_{\mathrm{i}3,\mathrm{f}3}=0, \quad (39)$$

$$C_\mathrm{i,f}=1, \quad \tau_2''=\tau_2, \quad \tau_1=\tau_2. \quad (40)$$

The matrix $\mathbf{\Psi}$ then reduces to the matrix given by Habicht *et al.* (2003). Since all elements of $\mathbf{T}$ except $T_1=-1$ are zero, the first term in equation (38) reduces to the basic expression $\tau''\mathbf{T}^\mathrm{T}\mathbf{J}=-\tau\Delta\omega$.

2.3. The τ dependence of the polarization

As a next step, we combine the SE Larmor phase with the TAS resolution function, first assuming an idealized sample with perfect lattice ($\Delta\mathbf{G}=0$) and a dispersion surface without curvature ($\mathbf{H}_0=0$). We allow for a detuning of the instrument, such that equations (3) and (4) are not satisfied. This will give us an expression for the polarization *versus* SE time τ according to equation (1). With these assumptions equation (38) reduces to

$$\Phi(\mathbf{k}_\mathrm{i},\mathbf{k}_\mathrm{f})-\Phi_0=\tau_2''\mathbf{T}^\mathrm{T}\mathbf{J}-\frac{1}{2}\tau_2''\mathbf{J}^\mathrm{T}\mathbf{\Psi}\mathbf{J}. \quad (41)$$

The TAS transmission function is described in terms of the matrix derived by Popovici (1975). In order to have a consistent nomenclature, the calculation of R_TAS is summarized in Appendix *A*. In terms of the variable vector $\mathbf{J}$ we get

$$R_\mathrm{TAS}(\mathbf{k}_\mathrm{i},\mathbf{k}_\mathrm{f})=\exp\left(-\frac{1}{2}\mathbf{J}^\mathrm{T}\mathbf{L}_\mathrm{TAS}\mathbf{J}\right). \quad (42)$$

Substituting equations (41) and (42) into the fundamental equation (1) gives

$$P=\frac{1}{N}\int S(\mathbf{Q},\omega)\exp\left(i\tau_2''\mathbf{T}^\mathrm{T}\mathbf{J}\right)\exp\left(-\frac{1}{2}\mathbf{J}^\mathrm{T}\mathbf{L}_\mathrm{I}\mathbf{J}\right)\mathrm{d}^6J_n$$

with

$$\mathbf{L}_\mathrm{I}=\mathbf{L}_\mathrm{TAS}+i\tau_2''\mathbf{\Psi}. \quad (43)$$

We now argue that all terms that are nonlinear in $\Delta\omega$ can be neglected in equation (43). The reason is that in SE measurements the energy width of $S(\Delta\omega)$ is much narrower than the energy width of the TAS transmission function R_TAS, and the range of $\Delta\omega$ is small, such that the integral in equation (43) is dominated by a term $\exp(-i\tau\Delta\omega)$. If both widths were comparable, it would make more sense to perform TAS scans to determine $S(\omega)$ without using SE. Neglecting terms nonlinear in $\Delta\omega$, equation (43) splits into a product of the resolution function and the Fourier transform of $S(\omega)$:

$$P = \frac{1}{N}\int S(\mathbf{Q},\omega)\exp(-i\tau_2''\Delta\omega)\,\mathrm{d}\Delta\omega \times \int \exp\left(i\tau_2''\widetilde{\mathbf{T}}^{\mathrm{T}}\widetilde{\mathbf{J}}\right)\exp\left(-\frac{1}{2}\widetilde{\mathbf{J}}^{\mathrm{T}}\widetilde{\mathbf{L}}_{\mathrm{I}}\widetilde{\mathbf{J}}\right)\mathrm{d}^5 J_n, \quad (44)$$

where $\widetilde{\mathbf{J}} = (\Delta k_{\mathrm{in}}, y_1, y_2, z_1, z_2)$ and $\widetilde{\mathbf{T}}$ are the five-dimensional subvectors of $\mathbf{J}$ and $\mathbf{T}$ without $\Delta\omega$. $\widetilde{\mathbf{L}}_{\mathrm{I}}$ is the corresponding symmetric (5×5) submatrix of $\mathbf{L}_{\mathrm{I}}$. The Gaussian resolution integral in equation (44) has the following general solution (Miller, 1964):

$$\int_{-\infty}^{\infty}\exp\left(\mathbf{K}^{\mathrm{T}}\mathbf{J}\right)\exp\left(-\frac{1}{2}\mathbf{J}^{\mathrm{T}}\mathbf{M}\mathbf{J}\right)\mathrm{d}^n\mathbf{J}_n = \frac{(2\pi)^{n/2}}{(\det\mathbf{M})^{1/2}}\exp\left(-\frac{1}{2}\mathbf{K}^{\mathrm{T}}\mathbf{M}^{-1}\mathbf{K}\right). \quad (45)$$

The second integral in equation (44), the resolution function, then reads

$$F_{\mathrm{I}}(\tau_2'') = \left|\left[\frac{\det\widetilde{\mathbf{L}}_{\mathrm{I}}(\tau_2''=0)}{\det\widetilde{\mathbf{L}}_{\mathrm{I}}(\tau_2'')}\right]^{1/2}\exp\left[-\frac{1}{2}\tau_2''^2\widetilde{\mathbf{T}}^{\mathrm{T}}\widetilde{\mathbf{L}}_{\mathrm{I}}^{-1}(\tau_2'')\widetilde{\mathbf{T}}\right]\right|. \quad (46)$$

The exponential term is unity for a tuned instrument, since in this case $\widetilde{\mathbf{T}}$ is zero and $F_{\mathrm{I}}(\tau_2'')$ then is identical to equation (65) in the work of Habicht *et al.* (2003). For strong detuning, this exponential term will dominate the decay of the polarization.

2.4. Sample mosaic and spread in *d* spacing

Mosaicity and spread of d spacing of the sample crystal lead to a variation of the direction and magnitude of the reciprocal-lattice vector $\Delta\mathbf{G} = \mathbf{G} - \mathbf{G}_0$, where $\mathbf{G}_0$ is the mean reciprocal-lattice vector corresponding to a perfect crystal. This also leads to a smearing of the effective excitation momentum $\Delta\mathbf{q} = \mathbf{Q}_0 - \Delta\mathbf{G}$. As a consequence, the SE phase in equation (38) gets the additional term $+\tau_2''\Delta\mathbf{G}\cdot\nabla\omega(\mathbf{q}_0)$. For a quantitative treatment we define the vertical ($\Delta\nu$) and horizontal ($\Delta\eta$) mosaicity and the variation of the magnitude ΔG:

$$\mathbf{G} = \mathbf{G}_0 + \Delta\mathbf{G} = \begin{bmatrix}(G_0+\Delta G)\cos\Delta\nu\cos\Delta\eta\\(G_0+\Delta G)\cos\Delta\nu\sin\Delta\eta\\(G_0+\Delta G)\sin\Delta\nu\end{bmatrix}. \quad (47)$$

We assume that the variations are small and expand to second order:

$$\Delta\mathbf{G} = \begin{bmatrix}\Delta G - \frac{1}{2}G_0(\Delta\nu^2+\Delta\eta^2)\\G_0\Delta\eta + \Delta G\Delta\eta\\G_0\Delta\nu + \Delta G\Delta\nu\end{bmatrix}. \quad (48)$$

Since for phonons the scattering cross section is proportional to $(\mathbf{Q}\cdot\boldsymbol{\xi})^2$ where $\boldsymbol{\xi}$ is the phonon polarization vector, $\mathbf{q}_0$ should ideally be perpendicular and parallel to $\mathbf{G}_0$ for the measurement of transverse and longitudinal phonons, respectively. Equation (48) shows that first-order contributions to the SE phase are linear in ΔG for longitudinal and linear in $\Delta\eta$ for transverse phonons. For the further calculation we separate linear and quadratic terms:

$$\Delta\mathbf{G}_{\mathrm{c}}' = \begin{pmatrix}\Delta G\\G_0\Delta\eta\\G_0\Delta\nu\end{pmatrix} \quad\text{and}\quad \Delta\mathbf{G}'' = \begin{bmatrix}-\frac{1}{2}G_0(\Delta\nu^2+\Delta\eta^2)\\\Delta G\Delta\eta\\\Delta G\Delta\nu\end{bmatrix}. \quad (49)$$

The complex resolution matrix including $\Delta\mathbf{G}$ reads

$$\mathbf{L}_{\mathrm{M}} = \mathbf{I}^{-1}\mathbf{L}_{\mathrm{I}}\mathbf{I} + \mathbf{N} + \mathbf{W} \quad (50)$$

with the nonzero elements of the (6×9) matrix $\mathbf{I}$

$$I_{11} = I_{22} = I_{33} = I_{44} = I_{55} = I_{66} = 1, \quad (51)$$

$$I_{17} = C_x, \quad I_{18} = C_y G_0, \quad I_{19} = C_z G_0, \quad (52)$$

and with the definition $\mathbf{C} = \nabla_{\mathbf{q}}\omega(\mathbf{q}_{\mathrm{c}0})$. The nonzero elements of the (9×9) matrix $\mathbf{N}$ are

$$N_{77} = \frac{1}{\Upsilon_{\mathrm{S}}^2}, \quad N_{88} = \frac{1}{\eta_{\mathrm{S}}^2}, \quad N_{99} = \frac{1}{\nu_{\mathrm{S}}^2}. \quad (53)$$

We assume a Gaussian distribution of ΔG, $\Delta\eta$ and $\Delta\nu$ with related standard deviations Υ_{S}, η_{S} and ν_{S}, respectively. The quadratic terms are taken into account by the symmetric (9×9) matrix $\mathbf{W}$ with the following nonzero elements:

$$W_{78} = W_{87} = -i\tau_2''C_y, \quad W_{79} = W_{97} = -i\tau_2''C_z, \quad (54)$$

$$W_{88} = +i\tau_2''C_x G_{0\mathrm{c}}, \quad W_{99} = +i\tau_2''C_x G_{0\mathrm{c}}. \quad (55)$$

Note that equation (54) is the corrected version of equation (83) in the work of Habicht *et al.* (2003). The linear terms in $\Delta\eta$, $\Delta\nu$ and ΔG_{c} arising from $\Delta\mathbf{G}_{\mathrm{c}}'$ can be written as $+i\tau_2''\mathbf{T}_g^{\mathrm{T}}\mathbf{J}_{\mathrm{M}}$, with the column vectors

$$\mathbf{T}_g = (0,0,0,0,0,0,C_x,C_yG_{0\mathrm{c}},C_zG_{0\mathrm{c}}), \quad (56)$$

$$\mathbf{J}_{\mathrm{M}} = (\Delta\omega,\Delta k_{\mathrm{in}},y_1,y_2,z_1,z_2,\Delta G_{\mathrm{c}},\Delta\eta,\Delta\nu). \quad (57)$$

All linear terms can be taken into account by introducing

$$\mathbf{T}_{\mathrm{M}} = \begin{bmatrix}-1, N_{\mathrm{I}}\left(C_{\mathrm{i}} - \dfrac{\tau_1}{\tau_2}C_{\mathrm{f}}\right), \dfrac{N_{\mathrm{I}}e_{\mathrm{i}2}}{\cos\theta_1}, -\dfrac{N_{\mathrm{F}}e_{\mathrm{f}2}}{\cos\theta_2},\\ N_{\mathrm{I}}e_{\mathrm{i}3}, -N_{\mathrm{F}}e_{\mathrm{f}3}, C_x, -C_yG_{0\mathrm{c}}, -C_zG_{0\mathrm{c}}\end{bmatrix}. \quad (58)$$

Analogous to the treatment in the previous subsection, terms in $\Delta\omega$ higher than linear are neglected, leading to

$$P = \frac{1}{N}\int S(\mathbf{Q},\omega)\exp(-i\tau_2''\Delta\omega)\,\mathrm{d}\Delta\omega \times \int \exp(i\tau_2''\widetilde{\mathbf{T}}_{\mathrm{M}}^{\mathrm{T}}\widetilde{\mathbf{J}}_{\mathrm{M}})\exp\left(-\frac{1}{2}\widetilde{\mathbf{J}}_{\mathrm{M}}^{\mathrm{T}}\widetilde{\mathbf{L}}_{\mathrm{M}}\widetilde{\mathbf{J}}_{\mathrm{M}}\right)\mathrm{d}^8 J_n, \quad (59)$$

where $\widetilde{\mathbf{J}}_{\mathrm{M}} = (\Delta k_{\mathrm{in}},y_1,y_2,z_1,z_2,\Delta G_{\mathrm{c}},\Delta\eta,\Delta\nu)$ and $\widetilde{\mathbf{T}}_{\mathrm{M}}$ are the eight-dimensional subvectors of $\mathbf{J}_{\mathrm{M}}$ and $\mathbf{T}_{\mathrm{M}}$, respectively. $\widetilde{\mathbf{L}}_{\mathrm{M}}$ is the corresponding symmetric (8×8) submatrix of $\mathbf{L}_{\mathrm{M}}$. The second integral is the resolution function. Integration using equation (45) gives

$$F_{\mathrm{M}}(\tau_2'') = \left|\left[\frac{\det\widetilde{\mathbf{L}}_{\mathrm{M}}(\tau_2''=0)}{\det\widetilde{\mathbf{L}}_{\mathrm{M}}(\tau_2'')}\right]^{1/2}\exp\left[-\frac{1}{2}\tau_2''^2\widetilde{\mathbf{T}}_{\mathrm{M}}^{\mathrm{T}}\widetilde{\mathbf{L}}_{\mathrm{M}}^{-1}(\tau_2'')\widetilde{\mathbf{T}}_{\mathrm{M}}\right]\right|. \quad (60)$$

2.5. Curvature of the dispersion surface

In this section the influence of the curvature of the dispersion surface on the Larmor phase is discussed. The planes of constant Larmor phase (Fig. 2) are usually tuned to be tangential to the dispersion surface, but a curvature of the surface leads to a smearing of the phase. As the dispersion surface is only visible within the volume of the resolution ellipsoid, we again use a second-order expansion employing the Hessian matrix:

$$H_{ij} = \frac{\partial^2}{\partial q_i \partial q_j}\omega(\mathbf{q}) \quad i,j = 1,2,3. \tag{61}$$

Within the resolution formalism, the matrix $\mathbf{H}$ is expressed in Cartesian coordinates related to the reciprocal lattice by the $\mathbf{B}$ matrix (Busing & Levy, 1967). If the Hessian matrix is calculated in reciprocal-lattice coordinates as $\mathbf{H}_{HKL}$ with basis vectors $\mathbf{b}_1 = \mathbf{a}^\star$, $\mathbf{b}_2 = \mathbf{b}^\star$ and $\mathbf{b}_3 = \mathbf{c}^\star$, then the transformation to Cartesian coordinates reads $\mathbf{H} = \mathbf{B}\mathbf{H}_{HKL}\mathbf{B}^{-1}$.

Following Habicht *et al.* (2003), the modified matrix reads

$$\mathbf{L}_\mathrm{C} = \mathbf{L}_\mathrm{I} + i\tau_2''\mathbf{I}_\mathrm{C}^{-1}\mathbf{\Theta}_\mathrm{C}^{-1}\mathbf{H}\mathbf{\Theta}_\mathrm{C}\mathbf{I}_\mathrm{C} \tag{62}$$

where the matrix $\mathbf{\Theta}_\mathrm{C}\mathbf{I}_\mathrm{C}$ transforms the Hessian $\mathbf{H}$ to the coordinate space of $\mathbf{L}_\mathrm{I}$. The matrix $\mathbf{\Theta}_\mathrm{C}$ describes the transformation

$$\Delta\mathbf{q}_\theta = \mathbf{\Theta}_\mathrm{C}\mathbf{Y} \tag{63}$$

with the column vector $\mathbf{Y} = (x_1, y_1, z_1, x_2, y_2, z_2)$ and its components defined in equations (8) and (9). The variation of the wavevector $\Delta\mathbf{q}_\theta = \Delta\mathbf{k}_\mathrm{i} - \Delta\mathbf{k}_\mathrm{f}$ is expressed in the basis of the Cartesian system ($\mathbf{i}_0$, $\mathbf{j}_0$ and $\mathbf{l}_0$). In this coordinate system the wavevector $\mathbf{Q}_\theta = (Q\,0\,0)$ is parallel to $\mathbf{i}_0$ (see Fig. 1). ($\mathbf{i}_0$, $\mathbf{j}_0$ and $\mathbf{l}_0$) are identical to the coordinate system defined as the θ system by Lumsden *et al.* (2005). In order to express $\Delta\mathbf{q}_\theta$ in the θ system, $\Delta\mathbf{k}_\mathrm{i}$ and $\Delta\mathbf{k}_\mathrm{f}$ are rotated into the $\mathbf{Q}_\theta$ frame. Using equations (8) and (9) and the definitions in Fig. 1 gives

$$\Delta\mathbf{k}_\mathrm{i} = (x_1\cos\varphi - y_1\sin\varphi)\mathbf{i}_0 + (x_1\sin\varphi + y_1\cos\varphi)\mathbf{j}_0 + z_1\mathbf{l}_0, \tag{64}$$

$$\Delta\mathbf{k}_\mathrm{f} = (x_2\cos\Xi - y_2\sin\Xi)\mathbf{i}_0 + (x_2\sin\Xi + y_1\cos\Xi)\mathbf{j}_0 + z_2\mathbf{l}_0, \tag{65}$$

where φ is defined as the angle between $\mathbf{Q}_\theta$ and $\mathbf{k}_\mathrm{i}$, and Ξ is defined as the angle between $\mathbf{Q}_\theta$ and $\mathbf{k}_\mathrm{f}$. Thus, for equation (63) to hold we obtain

$$\mathbf{\Theta}_\mathrm{C} = \begin{pmatrix} \cos\varphi & -\sin\varphi & 0 & -\cos\Xi & \sin\Xi & 0 \\ \sin\varphi & \cos\varphi & 0 & -\sin\Xi & -\cos\Xi & 0 \\ 0 & 0 & 1 & 0 & 0 & -1 \end{pmatrix}. \tag{66}$$

The definitions of φ and Ξ are different from those given by Habicht *et al.* (2003) and sign errors are corrected. In order to evaluate the expression $\Delta\mathbf{q}^\mathrm{T}\mathbf{H}\Delta\mathbf{q}$, the Hessian $\mathbf{H}$ first is rotated to $\mathbf{H}_\theta$. According to Lumsden *et al.* (2005) the transform of the vector $\mathbf{Q}$ is defined as

$$\mathbf{Q}_\theta = \mathbf{\Omega}\mathbf{M}\mathbf{N}\mathbf{U}\mathbf{B}\mathbf{Q} \tag{67}$$

and that of the matrix $\mathbf{H}$ is

$$\mathbf{H}_\theta = \mathbf{\Omega}\mathbf{M}\mathbf{N}\mathbf{U}\mathbf{B}\mathbf{H}\mathbf{B}^{-1}\mathbf{U}^{-1}\mathbf{N}^{-1}\mathbf{M}^{-1}\mathbf{\Omega}^{-1}. \tag{68}$$

Equation (68) is the generalization of the matrix transform given by equation (91) in the work of Habicht *et al.* (2003).

In order to evaluate the resolution matrix, the Hessian needs a further transformation into the variable space of the six-dimensional vector $\mathbf{J}$. The matrix $\mathbf{I}_\mathrm{C}$ relates $\mathbf{Y}$ and $\mathbf{J}$ by the linear transformation

$$\mathbf{Y} = \mathbf{I}_\mathrm{C}\mathbf{J}. \tag{69}$$

The aim is to obtain a linear relation between the variable vectors $\mathbf{J}$ and $\mathbf{Y}$. We start with the following expression [see equation (17)]:

$$\Delta\omega = N_\mathrm{I}\boldsymbol{\varepsilon}_\mathrm{i}\cdot\Delta\mathbf{k}_\mathrm{i} - N_\mathrm{F}\boldsymbol{\varepsilon}_\mathrm{f}\cdot\Delta\mathbf{k}_\mathrm{f}. \tag{70}$$

Substitution of $\mathbf{k}_{\mathrm{i,f}}$ and $\boldsymbol{\varepsilon}_{\mathrm{i,f}}$ by using equations (27), (28), (20) and (21) gives

$$\begin{aligned}\Delta\omega = {} & x_1(N_\mathrm{I}e_{\mathrm{i}1}\cos\theta_1 - N_\mathrm{I}e_{\mathrm{i}2}\sin\theta_1) \\ & + y_1(N_\mathrm{I}e_{\mathrm{i}1}\sin\theta_1 + N_\mathrm{I}e_{\mathrm{i}2}\cos\theta_1) + e_{\mathrm{i}3}N_\mathrm{I}z_1 \\ & - x_2(N_\mathrm{F}e_{\mathrm{f}1}\cos\theta_2 - N_\mathrm{F}e_{\mathrm{f}2}\sin\theta_2) \\ & - y_2(N_\mathrm{F}e_{\mathrm{f}1}\sin\theta_2 - N_\mathrm{F}e_{\mathrm{f}2}\cos\theta_2) - e_{\mathrm{f}3}N_\mathrm{F}z_2\end{aligned} \tag{71}$$

and

$$\Delta k_\mathrm{in} = x_1\cos\theta_1 + y_1\sin\theta_1. \tag{72}$$

According to equation (69) the transformation reads $\mathbf{J} = \mathbf{I}_\mathrm{C}^{-1}\mathbf{Y}$. The elements of the matrices $\mathbf{I}_\mathrm{C}^{-1}$ and $\mathbf{I}_\mathrm{C}$ are defined in Appendices *B*3 and *B*4. For tuned SE conditions equations (39) hold and $\mathbf{I}_\mathrm{C}$ reduces to the matrix given by Habicht *et al.* (2003).

With equations (69) and (63) the additional term in the Larmor phase due to a curved dispersion surface is given by

$$\begin{aligned}\Delta\mathbf{q}^\mathrm{T}\mathbf{H}\Delta\mathbf{q}_\mathrm{c} &= \mathbf{Y}^\mathrm{T}\mathbf{\Theta}_\mathrm{C}^{-1}\mathbf{H}\mathbf{\Theta}_\mathrm{C}\mathbf{Y} \\ &= \mathbf{J}^\mathrm{T}\mathbf{I}_\mathrm{C}^{-1}\mathbf{\Theta}_\mathrm{C}^{-1}\mathbf{H}\mathbf{\Theta}_\mathrm{C}\mathbf{I}_\mathrm{C}\mathbf{J}.\end{aligned} \tag{73}$$

The resolution matrix as given in equation (62) can now be evaluated. The polarization can again be written as a product of two integrals, where the second one is the resolution function:

$$\begin{aligned}P = {} & \frac{1}{N}\int S(\mathbf{Q},\omega)\exp(-i\tau_2''\Delta\omega)\,\mathrm{d}\Delta\omega \\ & \times \int \exp\left(i\tau_2''\widetilde{\mathbf{T}}^\mathrm{T}\widetilde{\mathbf{J}}\right)\exp\left(-\frac{1}{2}\widetilde{\mathbf{J}}^\mathrm{T}\widetilde{\mathbf{L}}_\mathrm{C}\widetilde{\mathbf{J}}\right)\mathrm{d}^5J_n.\end{aligned} \tag{74}$$

Using equation (45) the resolution function taking into account curvature effects (without including mosaicity and spread in d spacing) is

$$F_\mathrm{C}(\tau_2'') = \left|\left[\frac{\det\widetilde{\mathbf{L}}_\mathrm{C}(\tau_2''=0)}{\det\widetilde{\mathbf{L}}_\mathrm{C}(\tau_2'')}\right]^{1/2}\exp\left[-\frac{1}{2}\tau_2''^2\widetilde{\mathbf{T}}^\mathrm{T}\widetilde{\mathbf{L}}_\mathrm{C}^{-1}(\tau_2'')\widetilde{\mathbf{T}}\right]\right|. \tag{75}$$

2.6. Combining mosaicity, spread in *d* spacing and curvature of the dispersion surface

The results of the two previous sections can now be combined. The variation of the reciprocal-lattice vector $\Delta\mathbf{G}'$ [equation (49)] also requires $\Delta\mathbf{q}$ to be modified *via*

$$\Delta\mathbf{q}' = \Delta\mathbf{q} - \Delta\mathbf{G}', \tag{76}$$

which enters the curvature term

$$\begin{aligned}\Delta\mathbf{q}'^{\mathrm{T}}\mathbf{H}\Delta\mathbf{q}'_{\mathrm{c}} &= (\Delta\mathbf{q} - \Delta\mathbf{G}')^{\mathrm{T}}\mathbf{H}(\Delta\mathbf{q} - \Delta\mathbf{G}') \\ &= \Delta\mathbf{q}^{\mathrm{T}}\mathbf{H}\Delta\mathbf{q} + \Delta\mathbf{G}'^{\mathrm{T}}\mathbf{H}\Delta\mathbf{G}' \\ &\quad - 2\Delta\mathbf{q}^{\mathrm{T}}\mathbf{H}\Delta\mathbf{G}'. \end{aligned} \tag{77}$$

The corresponding matrix for the resolution function is

$$\mathbf{L}_{\mathrm{MC}} = \mathbf{I}^{\mathrm{T}}\mathbf{L}_{\mathrm{C}}\mathbf{I} + \mathbf{N} + \mathbf{W}. \tag{78}$$

The resolution function can be expressed as

$$F_{\mathrm{MC}}(\tau_2'') = \left|\left[\frac{\det\widetilde{\mathbf{L}}_{\mathrm{MC}}(\tau_2''=0)}{\det\widetilde{\mathbf{L}}_{\mathrm{MC}}(\tau_2'')}\right]^{1/2}\exp\left[-\frac{1}{2}\tau_2''^2\widetilde{\mathbf{T}}_{\mathrm{M}}^{\mathrm{T}}\widetilde{\mathbf{L}}_{\mathrm{MC}}^{-1}(\tau_2'')\widetilde{\mathbf{T}}_{\mathrm{M}}\right]\right|. \tag{79}$$

This resolution function F_{MC} includes lattice imperfections (mosaicity, spread of d spacing) and the curvature of the dispersion surface.

3. Energy detuning

In this section we calculate the effect of detuning both the TAS resolution ellipsoid and the SE parameters to a 'wrong' energy $\omega_{0\mathrm{TAS}}$, which does not coincide with the actual energy of the excitation ω_{0S} (see Fig. 3). Such a detuning might happen if the excitation energy is not known with sufficient precision or if there are multiple excitation branches within the TAS ellipsoid, so that tuning to all of these branches is not possible. In this section we assume that we have only one dispersion branch and that both the centre of the TAS ellipsoid and the nominal excitation share the same $\mathbf{q}_0$.

The shift in energy between the TAS resolution ellipsoid and the excitation is $\Delta\Omega_{\mathrm{TAS}} = \omega_{0\mathrm{TAS}}(\mathbf{q}_0) - \omega_{0S}(\mathbf{q}_0)$. We include this shift by substituting $\Delta\omega \rightarrow \Delta\omega - \Delta\Omega_{\mathrm{TAS}}$. The resolution matrix then reads

$$\begin{aligned}\mathbf{L}_{\mathrm{MC}} &= \mathbf{I}^{\mathrm{T}}\mathbf{L}_{\mathrm{C}}\mathbf{I} + \mathbf{N} + \mathbf{W} \\ &= \mathbf{I}^{\mathrm{T}}\left(\mathbf{L}_{\mathrm{TAS}} + i\tau_2''\boldsymbol{\Psi} + i\tau_2''\mathbf{I}_{\mathrm{C}}^{-1}\boldsymbol{\Theta}_{\mathrm{C}}^{-1}\mathbf{H}\boldsymbol{\Theta}_{\mathrm{C}}\mathbf{I}_{\mathrm{C}}\right)\mathbf{I} + \mathbf{N} + \mathbf{W}. \end{aligned} \tag{80}$$

Since only the TAS transmission function changes, the following substitution has to be made:

$$\mathbf{J}^{\mathrm{T}}\mathbf{I}^{\mathrm{T}}\mathbf{L}_{\mathrm{TAS}}\mathbf{I}\mathbf{J} \rightarrow \mathbf{J}_{\mathrm{TAS}}^{\mathrm{T}}\mathbf{I}^{\mathrm{T}}\mathbf{L}_{\mathrm{TAS}}\mathbf{I}\mathbf{J}_{\mathrm{TAS}} \tag{81}$$

with

$$\mathbf{J}_{\mathrm{TAS}} = \mathbf{J} - \mathbf{J}' = (\Delta\omega - \Delta\Omega_{\mathrm{TAS}}, \Delta k_{\mathrm{in}}, y_1, y_2, z_1, z_2). \tag{82}$$

The new TAS resolution matrix is defined as $\mathbf{L}_{\mathrm{S}} = \mathbf{I}^{\mathrm{T}}\mathbf{L}_{\mathrm{TAS}}\mathbf{I}$. The matrix $\mathbf{L}_{\mathrm{S}}$ is symmetric and therefore $\mathbf{J}'^{\mathrm{T}}\mathbf{L}_{\mathrm{S}}\mathbf{J} = \mathbf{J}^{\mathrm{T}}\mathbf{L}_{\mathrm{S}}\mathbf{J}'$. Using this symmetry yields

$$\begin{aligned}\mathbf{J}_{\mathrm{TAS}}^{\mathrm{T}}\mathbf{L}_{\mathrm{S}}\mathbf{J}_{\mathrm{TAS}} &= \mathbf{J}^{\mathrm{T}}\mathbf{L}_{\mathrm{S}}\mathbf{J} - 2\mathbf{J}^{\mathrm{T}}\mathbf{L}_{\mathrm{S}}\mathbf{J}' + \mathbf{J}'^{\mathrm{T}}\mathbf{L}_{\mathrm{S}}\mathbf{J}' \\ &= \mathbf{J}^{\mathrm{T}}\mathbf{L}_{\mathrm{S}}\mathbf{J} - 2\Delta\Omega_{\mathrm{TAS}}(\mathbf{L}_{\mathrm{S}})_{1n}\mathbf{J} \\ &\quad + (\mathbf{L}_{\mathrm{S}})_{11}\Delta\Omega_{\mathrm{TAS}}^2 \end{aligned} \tag{83}$$

where $(\mathbf{L}_{\mathrm{S}})_{1n}$ defines the six-dimensional row vector of the matrix $\mathbf{L}_{\mathrm{S}}$ and $(\mathbf{L}_{\mathrm{S}})_{11}$ is the (1, 1) element of the matrix $\mathbf{L}_{\mathrm{S}}$. The term proportional to $(\mathbf{L}_{\mathrm{S}})_{11}\Delta\Omega_{\mathrm{TAS}}^2$ is a constant, which can be absorbed in the normalization factor N. With

$$\begin{aligned}-\frac{1}{2}\mathbf{J}_{\mathrm{TAS}}^{\mathrm{T}}\mathbf{L}_{\mathrm{MC,TAS}}\mathbf{J}_{\mathrm{TAS}} &= -\frac{1}{2}\mathbf{J}^{\mathrm{T}}\mathbf{L}_{\mathrm{MC}}\mathbf{J} + \Delta\Omega_{\mathrm{TAS}}(\mathbf{L}_{\mathrm{S}})_{1n}\mathbf{J} \\ &\quad -\frac{1}{2}(\mathbf{L}_{\mathrm{S}})_{11}\Delta\Omega_{\mathrm{TAS}}^2 \end{aligned} \tag{84}$$

the modified expression for the polarization reads

$$\begin{aligned}P = \frac{1}{N}\int S(\mathbf{Q},\omega)\exp\left[-i\tau_2''\Delta\omega + \Delta\Omega_{\mathrm{TAS}}(\mathbf{L}_{\mathrm{S}})_{11}\Delta\omega\right]\mathrm{d}\Delta\omega \\ \times\int\exp\left(\widetilde{\mathbf{T}}_{\mathrm{TAS}}^{\mathrm{T}}\widetilde{\mathbf{J}}\right)\exp\left(-\frac{1}{2}\widetilde{\mathbf{J}}^{\mathrm{T}}\widetilde{\mathbf{L}}_{\mathrm{MC}}\widetilde{\mathbf{J}}\right)\mathrm{d}^5J_n. \end{aligned} \tag{85}$$

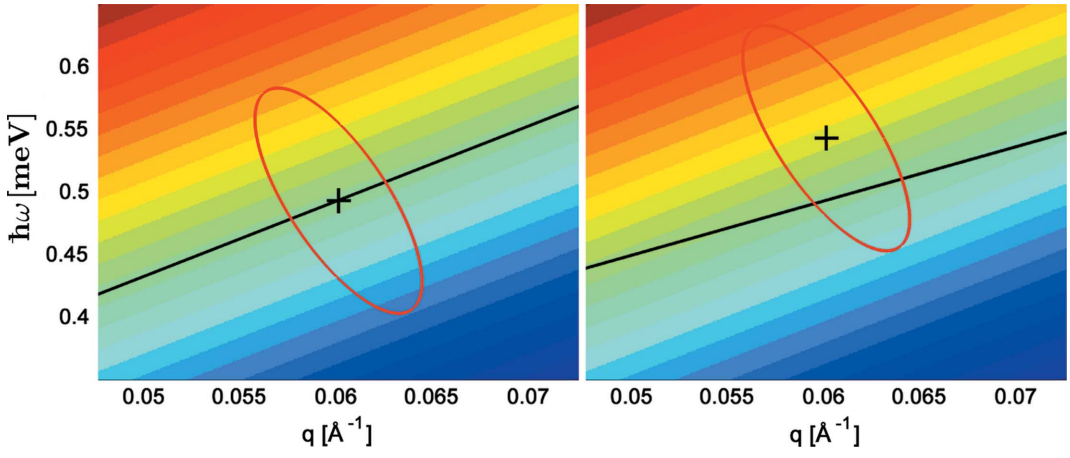

Figure 3
(Left) The lines of constant Larmor phase (here encoded by colours) are in the tuned case parallel to the dispersion surface (black line) and the TAS resolution ellipsoid is centred on the nominal excitation ($\mathbf{q}_0$, ω_0). (Right) The TAS ellipsoid is offset to ($\mathbf{q}_0$, $\omega_{0\mathrm{TAS}}$) and the lines of constant phase are detuned.

Here, the definition

$$\widetilde{\mathbf{T}}_{\rm TAS} = i\tau_2''\widetilde{\mathbf{T}}_{\rm M} + \Delta\Omega_{\rm TAS}(\widetilde{\mathbf{L}}_{\rm S})_{1n} \tag{86}$$

was used. The result for the resolution function, including its normalization to 1 at $\tau = 0$, reads then

$$\begin{aligned} F_{\rm MC,TAS}(\tau_2'') = \Bigg|\Bigg[\frac{\det\widetilde{\mathbf{L}}_{\rm MC}(\tau_2''=0)}{\det\widetilde{\mathbf{L}}_{\rm MC}(\tau_2'')}\Bigg]^{1/2} \\ \times \exp\Big[\frac{1}{2}\widetilde{\mathbf{T}}_{\rm TAS}^{\rm T}\widetilde{\mathbf{L}}_{\rm MC}^{-1}(\tau_2'')\widetilde{\mathbf{T}}_{\rm TAS}\Big] \\ \times \exp\Big[-\frac{1}{2}\widetilde{\mathbf{T}}_{\rm TAS}^{\rm T}(0)\widetilde{\mathbf{L}}_{\rm MC}^{-1}(\tau_2''=0)\widetilde{\mathbf{T}}_{\rm TAS}(0)\Big]\Bigg|. \end{aligned} \tag{87}$$

Since

$$\begin{aligned} \exp\Big(\widetilde{\mathbf{T}}_{\rm TAS}^{\rm T}\widetilde{\mathbf{L}}_{\rm MC}^{-1}\widetilde{\mathbf{T}}_{\rm TAS}\Big) = \exp\Big(-\tau_2''^2\widetilde{\mathbf{T}}_{\rm M}^{\rm T}\widetilde{\mathbf{L}}_{\rm MC}^{-1}\widetilde{\mathbf{T}}_{\rm M}\Big) \\ \times \exp\Big[+\Delta\Omega_{\rm TAS}^2(\widetilde{\mathbf{L}}_{\rm S})_{1n}^{\rm T}\widetilde{\mathbf{L}}_{\rm MC}^{-1}(\widetilde{\mathbf{L}}_{\rm S})_{1n}\Big] \\ \times \exp\Big[+i2\tau_2''\Delta\Omega_{\rm TAS}\widetilde{\mathbf{T}}_{\rm M}\widetilde{\mathbf{L}}_{\rm MC}^{-1}(\widetilde{\mathbf{L}}_{\rm S})_{1n}\Big] \end{aligned} \tag{88}$$

equation (87) yields

$$\begin{aligned} F_{\rm MC,TAS}(\tau_2'') = \Bigg|\Bigg[\frac{\det\widetilde{\mathbf{L}}_{\rm MC}(\tau_2''=0)}{\det\widetilde{\mathbf{L}}_{\rm MC}(\tau_2'')}\Bigg]^{1/2} \\ \times \exp\Big[\frac{1}{2}\Delta\Omega_{\rm TAS}^2(\widetilde{\mathbf{L}}_{\rm S})_{1n}^{\rm T}\widetilde{\mathbf{L}}_{\rm MC}^{-1}(\tau_2'')(\widetilde{\mathbf{L}}_{\rm S})_{1n}\Big] \\ \times \exp\Big[-\frac{1}{2}\Delta\Omega_{\rm TAS}^2(\widetilde{\mathbf{L}}_{\rm S})_{1n}^{\rm T}\widetilde{\mathbf{L}}_{\rm MC}^{-1}(\tau_2''=0)(\widetilde{\mathbf{L}}_{\rm S})_{1n}\Big] \\ \times \exp\Big[-\frac{1}{2}\tau_2''^2\widetilde{\mathbf{T}}_{\rm M}^{\rm T}\widetilde{\mathbf{L}}_{\rm MC}^{-1}(\tau_2'')\widetilde{\mathbf{T}}_{\rm M}\Big] \\ \times \exp\Big[i\tau_2''^2\Delta\Omega_{\rm TAS}\widetilde{\mathbf{T}}_{\rm M}^{\rm T}\widetilde{\mathbf{L}}_{\rm MC}^{-1}(\tau_2'')(\widetilde{\mathbf{L}}_{\rm S})_{1n}\Big]\Bigg|. \end{aligned} \tag{89}$$

Note that the phase term arising from

$$\begin{aligned} \exp\Big[-\frac{1}{2}\widetilde{\mathbf{T}}_{\rm TAS}^{\rm T}(0)\widetilde{\mathbf{L}}_{\rm MC}^{-1}(\tau_2''=0)\widetilde{\mathbf{T}}_{\rm TAS}(0)\Big] \\ = \exp\Big[-\frac{1}{2}\Delta\Omega_{\rm TAS}^2(\widetilde{\mathbf{L}}_{\rm S})_{1n}^{\rm T}\widetilde{\mathbf{L}}_{\rm MC}^{-1}(\tau_2''=0)(\widetilde{\mathbf{L}}_{\rm S})_{1n}\Big] \end{aligned} \tag{90}$$

can be neglected, since the term is independent of τ_2'' and thus is absorbed in the normalization factor.

The Fourier transform is no longer as simple as in the previous subsections, since there is an additional term linear in $\Delta\omega$:

$$\int \exp\big[\Delta\Omega_{\rm TAS}(\mathbf{L}_{\rm S})_{11}\Delta\omega\big]S(\Delta\omega)\exp(-i\tau_2''\Delta\omega)\,{\rm d}\Delta\omega. \tag{91}$$

The term $\exp[\Delta\Omega_{\rm TAS}(\mathbf{L}_{\rm S})_{11}\Delta\omega]$ introduces a small asymmetry. However, in practical cases $\Delta\Omega_{\rm TAS}(\mathbf{L}_{\rm S})_{11}\Delta\omega \ll 1$. Thus, the exponential $\exp[\Delta\Omega_{\rm TAS}(\mathbf{L}_{\rm S})_{11}\Delta\omega]$ only varies slowly with $\Delta\omega$ and close to 1 over the $\Delta\omega$ range of the scattering function $S(\Delta\omega)$. Therefore, this factor is neglected.

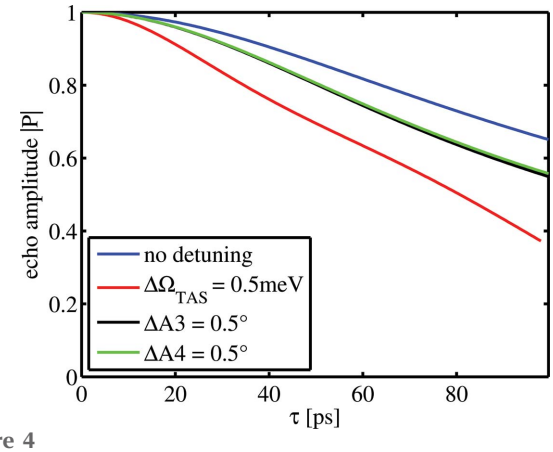

Figure 4
Depolarization effects for $RbMnF_3$ at the zone boundary excitation $Q = [0.5\,0.5\,-1]$, $\hbar\omega = 8.3$ meV, for energy detuned by $\Delta\Omega_{\rm TAS}$, crystal rotation angle detuned by ΔA3 and scattering angle detuned by ΔA4. The intrinsic magnon line width is assumed to be zero. The depolarization of the blue curve (no detuning) results from curvature effects.

Fig. 4 shows a numerical example for equation (89) for a zone boundary magnon in $RbMnF_3$, where an energy detuning by $\Delta\Omega_{\rm TAS}$, a crystal rotation angle detuning ΔA3 and a scattering angle detuning by ΔA4 are compared. The intrinsic magnon line width is assumed to be zero. The depolarization of the blue curve (labelled 'no detuning') results from curvature effects. In general, the effect of individually detuned parameters depends on the dispersion (energy, slope, curvature) and on the TAS configuration. In the case of a zone boundary excitation as in Fig. 4 with zero slope of the dispersion, the detuning in energy has the largest effect on the polarization, whereas detuning in A3 and A4 causes $\mathbf{q}_0$ to vary around the maximum of the dispersion, which only leads to small additional variations of the energy and the slope, such that the effect on the polarization is also small.

4. Two dispersion branches

Now we generalize the result of the previous section to the case of two dispersion branches within the volume of the resolution ellipsoid. A less general case has already been treated by Habicht *et al.* (2010), where, as simplification, the spectrometer was tuned to one excitation branch and detuned with respect to the second one. In the following calculation we allow for tuning to an arbitrary $\omega_{\rm TAS}$, which is more realistic compared with the experiment where the resolution ellipsoid is centred between the mode energies. We assume the TAS ellipsoid is centred at $(\mathbf{q}_0, \omega_{0\rm TAS})$, and that the energies of the two excitation branches at the same $\mathbf{q}_0$ are $\omega_{0S1}(\mathbf{q}_0)$ and $\omega_{0S2}(\mathbf{q}_0)$. The general expression for the polarization is given by

$$\begin{aligned} P = \frac{1}{N}\Bigg\{\int S_1(\mathbf{Q},\omega)R_1(\mathbf{k}_{\rm i},\mathbf{k}_{\rm f})\exp[i\Phi_1(\mathbf{k}_{\rm i},\mathbf{k}_{\rm f})]\,{\rm d}^3k_{\rm i}\,{\rm d}^3k_{\rm f} \\ + \int S_2(\mathbf{Q},\omega)R_2(\mathbf{k}_{\rm i},\mathbf{k}_{\rm f})\exp[i\Phi_2(\mathbf{k}_{\rm i},\mathbf{k}_{\rm f})]\,{\rm d}^3k_{\rm i}\,{\rm d}^3k_{\rm f}\Bigg\}. \end{aligned} \tag{92}$$

Using the results from the previous section P reads

$$P = \frac{1}{N}\left\{\int S_1(\Delta\omega)R_{\rm TAS}(\Delta\omega - \Delta\Omega_1, \widetilde{\mathbf{J}}_n) \times \exp[i\Phi_1(\Delta\omega, \widetilde{\mathbf{J}}_n)]\,{\rm d}\Delta\omega\,{\rm d}^5\widetilde{J}_n + \int S_2(\Delta\omega)R_{\rm TAS}(\Delta\omega - \Delta\Omega_2, \widetilde{\mathbf{J}}_n) \times \exp[i\Phi_2(\Delta\omega, \widetilde{\mathbf{J}}_n)]\,{\rm d}\Delta\omega\,{\rm d}^5\widetilde{J}_n\right\}, \quad (93)$$

where

$$\Delta\Omega_{1,2} = \omega_{0\rm TAS} - \omega_{0S1,0S2}(\mathbf{q}_{c0}). \quad (94)$$

The scattering function does not include the energy offsets:

$$S_{1,2}(\Delta\omega) = A_{1,2}\frac{\Gamma_{1,2}}{\Gamma_{1,2}^2 + \Delta\omega^2}. \quad (95)$$

Substituting the TAS resolution function $R_{\rm TAS}$ in equation (93), the most general case reads

$$P = \frac{1}{N}\left\{\int S_1(\Delta\omega)\exp\left[-i\tau''_{2,1}\Delta\omega + \Delta\Omega_1(\mathbf{L}_{\rm S})_{11}\Delta\omega\right]{\rm d}\Delta\omega \times \int \exp\left(\widetilde{\mathbf{T}}^{\rm T}_{\rm TAS1}\widetilde{\mathbf{J}}\right)\exp\left(-\frac{1}{2}\widetilde{\mathbf{J}}^{\rm T}\widetilde{\mathbf{L}}_{\rm MC1}\widetilde{\mathbf{J}}\right){\rm d}^5J_n + \int S_2(\Delta\omega)\exp\left[-i\tau''_{2,2}\Delta\omega + \Delta\Omega_2(\mathbf{L}_{\rm S})_{11}\Delta\omega\right]{\rm d}\Delta\omega \times \int \exp\left(\widetilde{\mathbf{T}}^{\rm T}_{\rm TAS2}\widetilde{\mathbf{J}}\right)\exp\left(-\frac{1}{2}\widetilde{\mathbf{J}}^{\rm T}\widetilde{\mathbf{L}}_{\rm MC2}\widetilde{\mathbf{J}}\right){\rm d}^5J_n\right\}, \quad (96)$$

where

$$\widetilde{\mathbf{T}}_{\rm TAS1,2} = i\tau''_{2,1,2}\widetilde{\mathbf{T}}_{\rm M1,2} + \Delta\Omega_{1,2}(\widetilde{\mathbf{L}}_{\rm S})_{1n}. \quad (97)$$

Generalizing the equation to more than two dispersion branches is possible in the same way, but is probably not of practical importance.

We tested this model by re-analysing experimental data on a zone boundary magnon in $RbMnF_3$ (Habicht *et al.*, 2010). The crystal consisted of two grains of comparable size and known relative orientation: one grain was oriented with the (*HHL*) plane parallel to the scattering plane, and the second grain was tilted about 10° out of this plane. The magnon branches of the two grains are very close at the zone boundary point $\mathbf{Q} = [0.5\,0.5\,-1]$, E = 8.46 meV, shown in Fig. 5, with a splitting of 0.4 meV calculated with the **UB** matrix formalism. The black line shows equation (96). The only free fitting parameter was the initial polarization $P(\tau = 0)$. The latter depends on the ratio of spin-flip and non-spin-flip processes, which also results from the unknown domain populations. [For isotropic domain populations one would expect $P(\tau = 0) = 0.5$.] Also included in the analysis is the effect of components of the gradient vector perpendicular to the scattering plane. Despite the large tilt of the second grain, these perpendicular components are small, as the gradient close to the zone boundary is also small. The discrepancy between the simple model ignoring the second mode and equation (96) is small in this example and only depends on one data point, but this example shows that the new model properly describes experimental data. The main feature in the black curve is an oscillation with a period $\Delta\tau \simeq 10$ ps, corresponding to the mode splitting $\Delta E = 2\pi\hbar/\Delta\tau \simeq 0.4$ meV.

Further experimental tests of the generalized resolution function have already been reported by Groitl *et al.* (2011). Here, a well defined model system to generate split excitation modes with variable splitting was used. The model system consisted of two Nb crystals both mounted in the (*HHL*) scattering plane, where one crystal could be rotated by a piezo drive around an axis perpendicular to the scattering plane (corresponding to an A3 rotation).

We first measured the SE amplitude $|P|$ *versus* τ for a transverse acoustic phonon at $\mathbf{Q}_0 = [1\,1\,0.05]$, E = 1.14 meV, using one single crystal. Data were collected at the FLEX spectrometer with NRSE (Keller *et al.*, 1995; Groitl *et al.*, 2015), using graphite (002) both as monochromator and

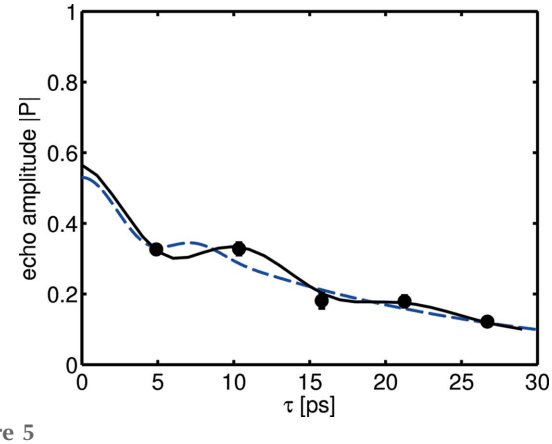

Figure 5
Experimental polarization data measured on a split boundary magnon $\mathbf{Q} = [0.5\,0.5\,-1]$, E = 8.46 meV, T = 3 K, in $RbMnF_3$ at TRISP (Habicht *et al.*, 2010). The black line shows the calculation according to the general model [equation (96)]. The simplified model assuming tuning to one branch (Habicht *et al.*, 2010) is shown as a dashed blue line.

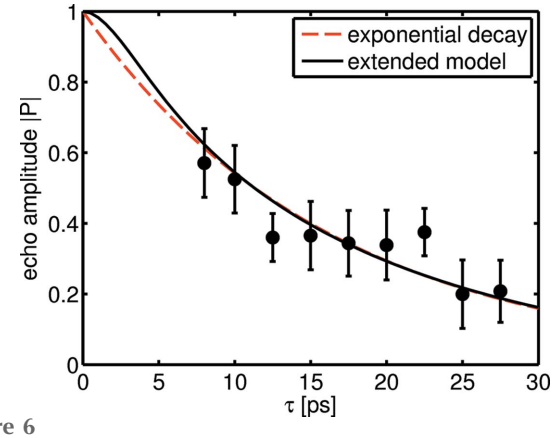

Figure 6
SE data for an acoustic phonon in a single Nb crystal at $\mathbf{Q}_0 = [1\,1\,0.05]$, E = 1.144 meV at T = 65 K (Groitl *et al.*, 2011). The simple exponential decay (red line) fitted with $P = \exp(-\Gamma\tau)$ gives Γ = 40 (3) μeV. A fit (black line) with equation (79) taking the curvature of the dispersion into account gives Γ = 2 (3) μeV, *i.e.* close to zero, as expected.

analyser, with $k_I = 1.90$ Å^{-1} (Groitl *et al.*, 2011; Groitl, 2012). The beam is polarized and analysed by transmission polarizers upstream of the monochromator and detector. At this small $q = 0.05$ reciprocal-lattice units (r.l.u.), corresponding to $q = 0.0968$ Å^{-1}, the dispersion surface is strongly curved ($\sim$500 meV Å^2) and significantly deviates from the planes of constant Larmor phase even for tuned SE parameters. The curvature induces a strong decay of $|P|$, which can be misinterpreted as intrinsic line width, as a fit with a simple exponential $\exp(-\Gamma\tau)$ gives a line width $\Gamma = 40\,(3)$ μeV (red dashed line in Fig. 6). The data were taken at a relatively low $T = 65$ K, where we expect an intrinsic phonon line width close to zero. A better fit using the resolution model, *i.e.* equation (79), requires us to model the dispersion surface locally around $\mathbf{q}_0$ to calculate the elements of the curvature matrix $\mathbf{H}_0$. We used the so-called DAF model (deLaunay, 1956) to parametrize the phonon dispersion of Nb. The result of a fit using equation (79) is shown as a black line in Fig. 6. The resulting line width $\Gamma = 2\,(3)$ μeV is, as expected, close to zero.

In order to test the resolution formalism for a mode doublet [equation (96)], we added the second Nb crystal on the above-mentioned sample holder and rotated it by 0.5° in the scattering plane with respect to the first one (corresponding to a rotation in A3). This corresponds to an offset in L by 0.012 r.l.u. and an energy splitting of 0.29 meV. This offset in q also induces components of the gradient vector perpendicular to the scattering plane, which were included in the analysis. The SE data in Fig. 7 show lower polarization than for the single crystal and a pronounced oscillation, where the modulation depth is given by the phonon intensities of the two crystals. For an analysis with the split mode resolution function [equation (96)] we used the same curvature matrix $\mathbf{H}_0$ as for the single dispersion in Fig. 6. As the NRSE setup at FLEX did not allow data collection at $\tau < 6$ ps, it proved difficult to fit Γ and $\Delta\Omega$ simultaneously. By assuming $\Gamma = 0$, as obtained for the single crystal, we get $\Delta\omega = 0.27\,(3)$ meV, in agreement with the calculated value.

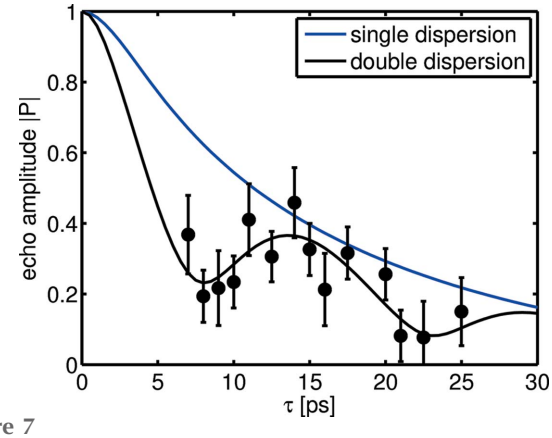

Figure 7
SE data on a model split mode generated by two mutually misaligned Nb crystals at $\mathbf{Q}_0 = [1\,1\,0.05]$ with a splitting $\Delta L = 0.012$ r.l.u. and corresponding $\Delta\Omega = 0.29$ meV (Groitl *et al.*, 2011). The black line shows a fit with the generalized resolution function [equation (96)]. The blue line shows for comparison the fit with equation (79) from Fig. 6.

5. Conclusion

The resolution model for SE-TASs developed here includes detuning effects and dispersion surfaces with components perpendicular to the scattering plane. The formalism works for arbitrary crystal symmetries. Curvature of the dispersion can be easily calculated in reciprocal-lattice units. These generalizations give more flexibility in the planning of experiments and data analysis. The compact matrix formalism allows for an easy numerical implementation.

APPENDIX *A*
TAS transmission function in matrix notation

The standard approximation of the resolution function for a conventional TAS has been derived (Cooper & Nathans, 1967) [corrections (Dorner, 1972)] and reformulated in a covariant matrix formalism (Stoica, 1975). The formalism has been extended (Popovici, 1975) to include real-space effects, such as finite spatial dimensions of the optical elements and the sample. Explicitly, the TAS resolution function reads (Popovici, 1975)

$$R_{\rm TAS}(\mathbf{X}) = \frac{R_0}{(2\pi)^2}(\det \mathbf{M}_{\rm TAS})^{1/2}\exp\left(-\frac{1}{2}\mathbf{X}^{\rm T}\mathbf{M}_{\rm TAS}\mathbf{X}\right) \quad (98)$$

with the four-component column vector $\mathbf{X} = (X_1, X_2, X_3, X_4) = [\mathbf{Q} - \mathbf{Q}_0, \omega(\mathbf{q}) - \omega_0(\mathbf{q}_0)]$. Note that X_4 is the fourth component of the vector $\mathbf{X}$ and the quantity $\Delta\omega = \omega(\mathbf{q}) - \omega_0(\mathbf{q})$ used in the calculations of the Larmor phase in NRSE experiments is different and refers to energy deviations from the dispersion surface for a given wavevector $\mathbf{q}$. $[R_0/(2\pi)^2](\det \mathbf{M}_{\rm TAS})^{1/2}$ is a normalization factor and R_0 is given in equation (16) in the work of Popovici (1975). Following Popovici the resolution matrix is given by

$$\mathbf{M}_{\rm TAS}^{-1} = \mathbf{BA}\left\{\left[\mathbf{D}(\mathbf{S} + \mathbf{T}^{\rm T}\mathbf{F}\mathbf{T})^{-1}\mathbf{D}^{\rm T}\right]^{-1} + \mathbf{G}\right\}^{-1}\mathbf{A}^{\rm T}\mathbf{B}^{\rm T}, \quad (99)$$

where $\mathbf{G}^{-1}$ is the covariance matrix of the distribution of the angular variables and $\mathbf{F}^{-1}$ is the covariance matrix of the reflectivity function. The matrices $\mathbf{A}, \mathbf{D}, \mathbf{S}, \mathbf{T}$ and $\mathbf{G}$ are defined as in Appendices I and II in the work of Popovici (1975). The linearized relation

$$\mathbf{X} = \mathbf{BY} \quad (100)$$

holds, with the six-component column vector $\mathbf{Y} = (\Delta\mathbf{k}_{\rm i}, \Delta\mathbf{k}_{\rm f})$ (see §2.5). In order to express the exponent of the resolution function as a function of the six-component column vector $\mathbf{J} = (\Delta\omega, \Delta k_{\rm in}, y_1, y_2, z_1, z_2)$, equation (69) is used with the 6×6 matrix $\mathbf{I}_{\rm C}$ as defined in Appendix *B*3. Therefore, equation (99) can be reformulated, yielding for the TAS resolution matrix in the frame of $\mathbf{J}$:

$$\mathbf{L}_{\rm TAS} = \left(\mathbf{I}_{\rm C}^{-1}\mathbf{A}\left\{\left[\mathbf{D}(\mathbf{S} + \mathbf{T}^{\rm T}\mathbf{F}\mathbf{T})^{-1}\mathbf{D}^{\rm T}\right]^{-1} + \mathbf{G}\right\}^{-1}\mathbf{A}^{\rm T}(\mathbf{I}_{\rm C}^{-1})^{\rm T}\right)^{-1}. \quad (101)$$

APPENDIX *B*
Matrix elements

B1. T vector

The components of the six-dimensional column vector **T** introduced in equation (38) are

$$T_1 = -1, \quad T_2 = N_\mathrm{I}\left(C_\mathrm{i} - \frac{\tau_1}{\tau_2} C_\mathrm{f}\right), \quad T_3 = \frac{N_\mathrm{I} e_{\mathrm{i}2}}{\cos\theta_1},$$
$$T_4 = -\frac{N_\mathrm{F} e_{\mathrm{f}2}}{\cos\theta_2}, \quad T_5 = N_\mathrm{I} e_{\mathrm{i}3}, \quad T_6 = -N_\mathrm{F} e_{\mathrm{f}3}. \tag{102}$$

B2. The Ψ matrix

The nonzero elements of the symmetric 6 × 6 matrix **Ψ** in equation (38) are

$$\Psi_{11} = -\frac{2D_2}{C_\mathrm{f}^2 N_\mathrm{F}^2 \tau_2''}, \tag{103}$$

$$\Psi_{22} = -\frac{\hbar}{m} - \frac{\hbar}{m}\tan^2\theta_1 - 2\frac{\tau_1}{\tau_2''}\frac{N_\mathrm{I}}{\mathbf{k}_\mathrm{I}\cdot\mathbf{n}_\mathrm{i}} - 2\frac{D_2}{\tau_2''}\frac{C_\mathrm{i}^2 N_\mathrm{I}^2}{C_\mathrm{f}^2 N_\mathrm{F}^2}, \tag{104}$$

$$\Psi_{33} = -\frac{\hbar}{m}\frac{1}{\cos^2\theta_1} - 2\frac{D_2}{\tau_2''}\frac{e_{\mathrm{i}2}^2 N_\mathrm{I}^2}{C_\mathrm{f}^2 N_\mathrm{F}^2}\frac{1}{\cos^2\theta_1}, \tag{105}$$

$$\Psi_{44} = \frac{\hbar}{m}\frac{1}{\cos^2\theta_2} + 2\frac{\hbar}{m}\frac{\tan\theta_2}{\cos^2\theta_2}\frac{1}{C_\mathrm{f}} e_{\mathrm{f}2} - 2\frac{D_2}{\tau_2''}\frac{e_{\mathrm{f}2}^2}{C_\mathrm{f}^2}\frac{1}{\cos^2\theta_2}, \tag{106}$$

$$\Psi_{55} = -\frac{\hbar}{m} - 2\frac{D_2}{\tau_2''}\frac{e_{\mathrm{i}3}^2 N_\mathrm{I}^2}{C_\mathrm{f}^2 N_\mathrm{F}^2}, \tag{107}$$

$$\Psi_{66} = \frac{\hbar}{m} - 2\frac{D_2}{\tau_2''}\frac{e_{\mathrm{f}3}^2}{C_\mathrm{f}^2}, \tag{108}$$

$$\Psi_{12} = 2\frac{D_2}{\tau_2''}\frac{C_\mathrm{i} N_\mathrm{I}}{C_\mathrm{f}^2 N_\mathrm{F}^2}, \tag{109}$$

$$\Psi_{13} = 2\frac{D_2}{\tau_2''}\frac{e_{\mathrm{i}2} N_\mathrm{I}}{C_\mathrm{f}^2 N_\mathrm{F}^2}\frac{1}{\cos\theta_1}, \tag{110}$$

$$\Psi_{14} = -2\frac{D_2}{\tau_2''}\frac{e_{\mathrm{f}2}}{C_\mathrm{f}^2 N_\mathrm{F}}\frac{1}{\cos\theta_2} + \frac{\hbar}{m}\frac{\tan\theta_2}{\cos\theta_2}\frac{1}{C_\mathrm{f} N_\mathrm{F}}, \tag{111}$$

$$\Psi_{15} = 2\frac{D_2}{\tau_2''}\frac{e_{\mathrm{i}3} N_\mathrm{I}}{C_\mathrm{f}^2 N_\mathrm{F}^2}, \tag{112}$$

$$\Psi_{16} = -2\frac{D_2}{\tau_2''}\frac{e_{\mathrm{f}3}}{N_\mathrm{F} C_\mathrm{f}^2}, \tag{113}$$

$$\Psi_{23} = \frac{\hbar}{m}\frac{\tan\theta_1}{\cos\theta_1} - 2\frac{D_2}{\tau_2''}\frac{C_\mathrm{i} N_\mathrm{I}^2}{C_\mathrm{f}^2 N_\mathrm{F}^2} e_{\mathrm{i}2}\frac{1}{\cos\theta_1}, \tag{114}$$

$$\Psi_{24} = -\frac{\hbar}{m}\frac{\tan\theta_2}{\cos\theta_2}\frac{C_\mathrm{i} N_\mathrm{I}}{C_\mathrm{f} N_\mathrm{F}} + 2\frac{D_2}{\tau_2''}\frac{C_\mathrm{i} N_\mathrm{I}}{C_\mathrm{f}^2 N_\mathrm{F}} e_{\mathrm{f}2}\frac{1}{\cos\theta_2}, \tag{115}$$

$$\Psi_{25} = -2\frac{D_2}{\tau_2''}\frac{C_\mathrm{i} N_\mathrm{I}^2}{C_\mathrm{f}^2 N_\mathrm{F}^2} e_{\mathrm{i}3}, \tag{116}$$

$$\Psi_{26} = 2\frac{D_2}{\tau_2''}\frac{C_\mathrm{i} N_\mathrm{I}}{C_\mathrm{f}^2 N_\mathrm{F}} e_{\mathrm{f}3}, \tag{117}$$

$$\Psi_{34} = 2\frac{D_2}{\tau_2''}\frac{e_{\mathrm{i}2} e_{\mathrm{f}2} N_\mathrm{I}}{C_\mathrm{f}^2 N_\mathrm{F}}\frac{1}{\cos\theta_1\cos\theta_2} - \frac{\hbar}{m}\frac{\tan\theta_2}{\cos\theta_2\cos\theta_1}\frac{N_\mathrm{I}}{C_\mathrm{f} N_\mathrm{F}} e_{\mathrm{i}2}, \tag{118}$$

$$\Psi_{35} = 0, \tag{119}$$

$$\Psi_{36} = -2\frac{D_2}{\tau_2''}\frac{e_{\mathrm{i}2} e_{\mathrm{i}3} N_\mathrm{I}^2}{C_\mathrm{f}^2 N_\mathrm{F}^2}\frac{1}{\cos\theta_1} + 2\frac{D_2}{\tau_2''}\frac{e_{\mathrm{i}2} e_{\mathrm{f}3} N_\mathrm{I}}{C_\mathrm{f}^2 N_\mathrm{F}}\frac{1}{\cos\theta_1}, \tag{120}$$

$$\Psi_{45} = 2\frac{D_2}{\tau_2''}\frac{e_{\mathrm{f}2} e_{\mathrm{i}3} N_\mathrm{I}}{C_\mathrm{f}^2 N_\mathrm{F}}\frac{1}{\cos\theta_2} - \frac{\hbar}{m}\frac{\tan\theta_2}{\cos\theta_2}\frac{1}{C_\mathrm{f}}\frac{N_\mathrm{I}}{N_\mathrm{F}} e_{\mathrm{i}3}, \tag{121}$$

$$\Psi_{46} = -2\frac{D_2}{\tau_2''}\frac{e_{\mathrm{f}2} e_{\mathrm{f}3}}{C_\mathrm{f}^2}\frac{1}{\cos\theta_2} + \frac{\hbar}{m}\frac{\tan\theta_2}{\cos\theta_2}\frac{1}{C_\mathrm{f}} e_{\mathrm{f}3}, \tag{122}$$

$$\Psi_{56} = 2\frac{D_2}{\tau_2''}\frac{e_{\mathrm{i}3} e_{f3} N_\mathrm{I}}{C_\mathrm{f}^2 N_\mathrm{F}}, \tag{123}$$

with

$$D_2 = \left(-\tau_2\frac{N_\mathrm{F}}{\mathbf{k}_\mathrm{F}\cdot\mathbf{n}_\mathrm{f}} - \frac{\hbar}{2m}\tau_2'' - \frac{\hbar}{2m}\tau_2''\tan^2\theta_2\right). \tag{124}$$

B3. The $\mathbf{I}_\mathrm{C}$ matrix

The nonzero elements of the 6 × 6 matrix $\mathbf{I}_\mathrm{C}$ in equation (73) are

$$I_{\mathrm{C},12} = \frac{1}{\cos\theta_1}, \tag{125}$$

$$I_{\mathrm{C},13} = -\tan\theta_1, \tag{126}$$

$$I_{\mathrm{C},41} = -\frac{1}{N_\mathrm{F} e_{\mathrm{f}2}\sin\theta_2 + N_\mathrm{F} e_{\mathrm{f}1}\cos\theta_2}, \tag{127}$$

$$I_{\mathrm{C},42} = -\frac{e_{\mathrm{i}2} N_\mathrm{I}\sin\theta_1 - e_{\mathrm{i}1} N_\mathrm{I}\cos\theta_1}{e_{\mathrm{f}1} N_\mathrm{F}\cos\theta_1\cos\theta_2 + e_{\mathrm{f}2} N_\mathrm{F}\cos\theta_1\sin\theta_2}, \tag{128}$$

$$I_{\mathrm{C},43} = \frac{e_{\mathrm{i}2} N_\mathrm{I}\cos^2\theta_1 + e_{\mathrm{i}2} N_\mathrm{I}\sin^2\theta_1}{e_{\mathrm{f}1} N_\mathrm{F}\cos\theta_1\cos\theta_2 + e_{\mathrm{f}2} N_\mathrm{F}\cos\theta_1\sin\theta_2}, \tag{129}$$

$$I_{\mathrm{C},44} = -\frac{e_{\mathrm{f}1}\sin\theta_2 - e_{\mathrm{f}2}\cos\theta_2}{e_{\mathrm{f}1}\cos\theta_2 + e_{\mathrm{f}2}\sin\theta_2}, \tag{130}$$

$$I_{\mathrm{C},45} = \frac{N_\mathrm{I} e_{\mathrm{i}3}}{e_{\mathrm{f}2} N_\mathrm{F}\sin\theta_2 + e_{\mathrm{f}1} N_\mathrm{F}\cos\theta_2}, \tag{131}$$

$$I_{\mathrm{C},46} = \frac{e_{\mathrm{f}3}}{e_{\mathrm{f}1}\cos\theta_2 + e_{\mathrm{f}2}\sin\theta_2}, \tag{132}$$

$$I_{\mathrm{C},23} = I_{\mathrm{C},35} = I_{\mathrm{C},54} = I_{\mathrm{C},66} = 1. \tag{133}$$

B4. The $\mathbf{I}_C^{-1}$ matrix

The nonzero elements of the 6×6 matrix $\mathbf{I}_C^{-1}$ in equation (73) are

$$I_{C,11}^{-1} = N_I(e_{i1}\cos\theta_1 - e_{i2}\sin\theta_1), \quad (134)$$

$$I_{C,12}^{-1} = N_I(e_{i1}\sin\theta_1 + e_{i2}\cos\theta_1), \quad (135)$$

$$I_{C,13}^{-1} = e_{i3}N_I, \quad (136)$$

$$I_{C,14}^{-1} = -N_F(e_{f1}\cos\theta_2 + e_{f2}\sin\theta_2), \quad (137)$$

$$I_{C,15}^{-1} = -N_F(e_{f1}\sin\theta_2 - e_{f2}\cos\theta_2), \quad (138)$$

$$I_{C,16}^{-1} = -e_{f3}N_F, \quad (139)$$

$$I_{C,21}^{-1} = \cos\theta_1, \quad (140)$$

$$I_{C,22}^{-1} = \sin\theta_1, \quad (141)$$

$$I_{C,32}^{-1} = I_{C,45}^{-1} = I_{C,53}^{-1} = I_{C,66}^{-1} = 1. \quad (142)$$

Acknowledgements

The authors would like to thank Mechthild Enderle, ILL, for valuable discussions.

References

Bayrakci, S., Keller, T., Habicht, K. & Keimer, B. (2006). *Science*, **312**, 1926–1929.
Busing, W. R. & Levy, H. A. (1967). *Acta Cryst.* **22**, 457–464.
Cooper, M. J. & Nathans, R. (1967). *Acta Cryst.* **23**, 357–367.
Dorner, B. (1972). *Acta Cryst.* A**28**, 319–327.
Gähler, R., Felber, J., Mezei, F. & Golub, R. (1998). *Phys. Rev. A*, **58**, 280–295.
Gähler, R. & Golub, R. (1988). *J. Phys. Fr.* **49**, 1195–1202.
Golub, R. & Gähler, R. (1987). *Phys. Lett. A*, **123**, 43–48.
Groitl, F. (2012). PhD thesis, TU Berlin, Germany.
Groitl, F., Keller, T., Quintero-Castro, D. L. & Habicht, K. (2015). *Rev. Sci. Instrum.* **86**, 025110.
Groitl, F., Kiefer, K. & Habicht, K. (2011). *Physica B*, **406**, 2342–2345.
Habicht, K. (2003). *Lecture Notes in Physics*, *Neutron Spin Echo Spectroscopy*, edited by F. Mezei, C. Pappas & T. Gutberlet, pp. 116–132. Berlin, Heidelberg: Springer.
Habicht, K., Enderle, M., Fåk, B., Hradil, K., Böni, P. & Keller, T. (2010). *J. Phys. Conf. Ser.* **211**, 012028.
Habicht, K., Golub, R., Mezei, F., Keimer, B. & Keller, T. (2004). *Phys. Rev. B*, **69**, 104301.
Habicht, K., Keller, T. & Golub, R. (2003). *J. Appl. Cryst.* **36**, 1307–1318.
Keller, T., Gähler, R., Kunze, H. & Golub, R. (1995). *Neutron News*, **6**, 16–17.
Keller, T., Golub, R. & Gähler, R. (2002). *Scattering*, edited by R. Sabatier & P. Pike, pp. 1264–1286. London: Academic Press.
Keller, T., Habicht, K., Golub, R. & Mezei, F. (2004). *Europhys. Lett.* **67**, 773–778.
Keller, T., Habicht, K., Klann, H., Ohl, M., Schneider, H. & Keimer, B. (2002). *Appl. Phys. A Mater. Sci. Process.* **74**, s332–s335.
Klimko, S., Stadler, C., Böni, P., Currat, R., Demmel, F., Fåk, B., Gähler, R., Mezei, F. & Toperverg, B. (2003). *Physica B*, **335**, 188–192.
Launay, J. de (1956). *Solid State Physics: Advances in Research and Applications.* Vol. 2, edited by F. Seitz, D. Turnbull & J. A. Cowen, pp. 219–303. New York: Academic Press.
Li, F., Feng, H., Thaler, A. N., Parnell, S. R., Hamilton, W. A., Crow, L., Yang, W., Jones, A. B., Bai, H., Matsuda, M., Baxter, D. V., Keller, T., Fernandez-Baca, J. A. & Pynn, R. (2017). *Sci. Rep.* **7**, 865.
Lumsden, M. D., Robertson, J. L. & Yethiraj, M. (2005). *J. Appl. Cryst.* **38**, 405–411.
Martin, N., Regnault, L.-P., Klimko, S., Lorenzo, J. E. & Gähler, R. (2011). *Physica B*, **406**, 2333–2336.
Mezei, F. (1978). *Neutron Inelastic Scattering*, p. 125. Vienna: IAEA.
Mezei, F. (1980). *Neutron Spin Echo*, Lecture Notes in Physics, Vol. 128. Berlin, Heidelberg: Springer.
Miller, K. (1964). *Multidimensional Gaussian Distributions.* SIAM Series in Applied Mathematics. New York: Wiley.
Popovici, M. (1975). *Acta Cryst.* A**31**, 507–513.
Shirane, G., Shapiro, S. & Tranquada, J. (2002). *Neutron Scattering with a Triple-Axis Spectrometer.* Cambridge University Press.
Stoica, A. D. (1975). *Acta Cryst.* A**31**, 189–192.